Chemiresistive Sensing with Chemically Modified Metal and Alloy Nanoparticles

Francisco J. Ibañez and Francis P. Zamborini*

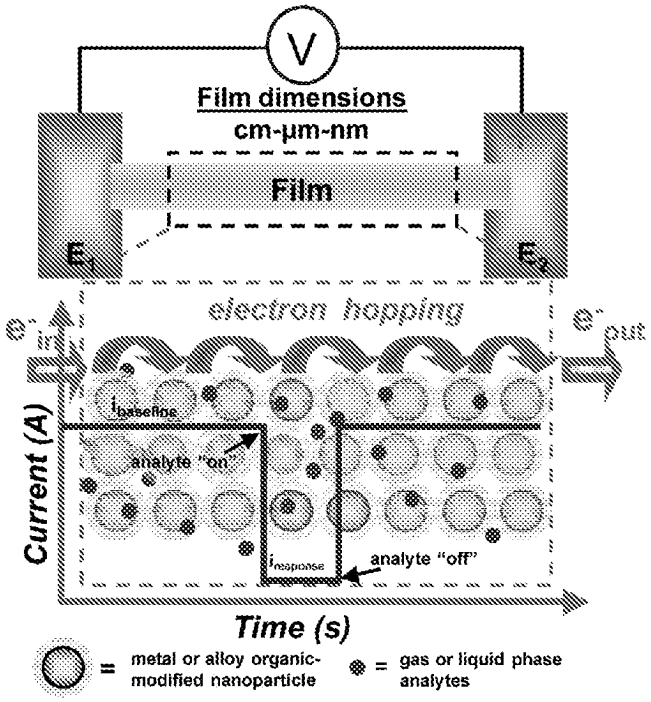

From the Contents

This review describes the use of chemically modified pure and alloyed metal nanoparticles for chemiresistive sensing applications. Chemically modified metal nanoparticles consist of a pure or alloyed metallic core with some type of chemical coating. Researchers have studied the electronic properties of 1D, 2D, and 3D assemblies of chemically modified metal nanoparticles, and even single individual nanoparticles. The interaction with the analyte alters the conductivity of the sensitive material, providing a signal to measure the analyte concentration. This review focuses on chemiresistive sensing of a wide variety of gas- and liquid-phase analytes with metal nanoparticles coated with organothiols, ions, polymers, surfactants, and biomolecules. Different strategies used to incorporate chemically modified nanoparticles into chemiresistive sensing devices are reviewed, focusing on the different types of metal and alloy compositions, coatings, methods of assembly, and analytes (vapors, gases, liquids, biological materials), along with other important factors.

small

1. Introduction

Chemiresistors are a class of sensing devices fabricated with a conductive or semiconductive material that exhibits a change in resistance when exposed to a chemical analyte of interest. As shown in **Figure 1**, this type of sensor consists of a chemically sensitive conductive film deposited between two metal electrodes. Upon application of a potential (V), there is a measurable current or resistance, R_1, across the film that changes to R_2 upon interaction with an analyte (A) of interest. Various types of materials have been used as the films in chemiresistors. Traditionally, these have included metals,[1] metal oxides,[2–5] conductive polymers,[6] and insulating polymers embedded with metal or carbon, such as carbon black/polymer composites.[7]

There are a variety of mechanisms that can lead to a resistance change in a material upon interaction with an analyte. When pure Pd metal interacts with hydrogen gas, for example, Pd hydride (PdH_x) forms, which has a larger resistance compared to Pd.[1,8] The resistance change can be used to detect hydrogen gas quantitatively. Metal oxides[2–5] are p- or n-type semiconductive materials whose charge carrier mobility is altered by the presence of oxidizing or reducing analytes, causing a change in the film resistance. Carbon black/polymer composites are hybrid materials with a conductive element (carbon black) and insulating organic polymer component.[7] Vapor phase analytes can partition into the polymer, which leads to film swelling and an increase in resistance based on a reduction in the conductive pathways through the carbon black. Sensor arrays comprised of several devices, each with a different type of polymer in the carbon black/polymer film, exhibit a different pattern of responses to different vapor phase analytes (usually volatile organic compounds, or VOCs). Pattern recognition methods, such as principal component analysis,[3,9–11] allow one to distinguish between the different analytes. This sensor array strategy used for the detection of gas or vapor phase molecules has been termed 'electronic noses'.[12–14]

Recently, nanomaterials have been widely explored for chemiresistive sensing applications.[15,16,19,108] Examples include metal or semiconducting nanowires,[5] carbon nanotubes,[16,17] fullerenes,[18] graphene,[19,20] and semiconductive or metallic nanoparticles.[2,21,31,35,39,49,67] The small size and high surface-to-volume ratio of nanoscale materials provides several benefits for sensing over more traditional bulk films. Since the surface atoms dominate the electronic properties of the nanomaterial, analyte interactions with the surface usually lead to much larger changes in resistance compared to bulk materials, providing lower detection limits. Analyte diffusion lengths are much smaller in nanoscale materials, leading to faster equilibration with the analyte and faster response times. Their small size results in a high level of device miniaturization, which leads to low cost, low power consumption, the possibility of performing fast measurements in the field, and ability to measure analyte in highly-confined spaces.

There are several published reviews that discuss the synthesis, fundamental properties, and applications of metal or metal oxide nanoparticles that are important, including those describing charge transport[22] and the electrochemistry[23] of nanoparticles and those describing applications in chemiresistive sensing,[2,24] catalysis,[25] chemical and biological sensing,[25] and medicine.[26] This review specifically focuses on the use of chemically modified metallic (pure and alloy) nanoparticles for chemiresitive sensing applications. Various metals have been employed, such as Au, Pt, Pd, Ag, and alloys of these metals. Several modifications of the metal nanoparticles have also been explored, including functionalization with organic self-assembled monolayers (SAMs), polymers, surfactants, ions, and biomolecules, depending on the sensing application. Section 2 of this review describes the different strategies for the synthesis and functionalization of metal nanoparticles that are commonly used for chemiresistive applications. After their synthesis, it is necessary to incorporate the modified metal nanoparticles into the chemiresistive device as 2D or 3D assemblies (or films), or even as individual nanoparticles in some cases. In Section 3, we briefly describe both the electrode device fabrication and assembly of the metal nanoparticles across the electrodes. In Section 4, we review electron transport through metal nanoparticle films and individual metal nanoparticles as this is important in understanding the chemiresistive sensing mechanism. In Section 5, we review analyte partitioning into the chemiresistive films, which is important in the description of any type of sensor. The analyte of interest can be gas phase or liquid phase organic, inorganic, or biological molecules. In Sections 6, 7, and 8, we review the various chemiresistive sensing applications for vapor-phase molecules, gases, and liquid-phase analytes, respectively. Finally, we summarize and discuss future directions of the field in Section 9.

Table 1 summarizes the different types of chemically modified metal and alloy nanoparticles discussed in this review. The table provides details about metal composition, size of the nanoparticles, organic coating, linker (if any), film-deposition method, sensing environment, types of analyte detected, limit of detection (LOD) for the indicated analyte, and current response direction. We made our best effort to include all articles relevant to this field in this review and apologize for any reports that we may have mistakenly overlooked.

2. Synthesis and Functionalization of Chemically Modified Metal Nanoparticles

2.1. Electrostatically Stabilized Metal Nanoparticles

The most common electrostatically-coated nanoparticles are those stabilized with negatively charged citrate ions

Dr. F. J. Ibañez
Instituto de Investigaciones Fisicoquímicas
Teóricas y Aplicadas (INIFTA)
Universidad Nacional de La Plata - CONICET
Sucursal 4 Casilla de Correo 16 (1900) La Plata, Argentina
E-mail: fjiban@inifta.unlp.edu.ar
Prof. F. P. Zamborini
Department of Chemistry
University of Louisville
Louisville, Kentucky 40292, USA

DOI: 10.1002/smll.201002232

synthesized following the Turkevich method.[60] Briefly, a metal ion precursor (usually $HAuCl_4$) is reduced in water by trisodium citrate at high temperature, which serves as both a reducing agent and weak stabilizer. This approach generally leads to nanoparticle diameters between 12 and 20 nm. The use of borohydride as a reductant in the presence of trisodium salt at room temperature, results in smaller nanoparticles ($d \approx 4$–5 nm), which are generally used as seed particles for subsequent growth in the presence of metal salt and surfactant to produce larger various-shaped nanoparticles, including rods, wires, triangles, cubes, and branched structures.[61,107,109] Electrostatically-stabilized metal nanoparticles have a large propensity to aggregate and it is difficult to directly form drop-cast films from them. For this reason, they are usually further treated in post-synthesis steps, including cross-linking reactions, place exchange reactions with other ligands, layer-by-layer film formation, and biomolecular functionalization.[62]

2.2. Surfactant or Polymer-Stabilized Metal Nanoparticles

Surfactant or polymer-stabilized nanoparticles have been recently synthesized and characterized with potential medical applications[63] and for chemiresistive sensing of vapor and gas analytes.[38,55] We previously synthesized tetraoctylammonium bromide (TOABr)-coated Au, Pd, AuAg, and PdAg nanoparticles by the reduction of $AuCl_4^-$, $PdCl_4^{2-}$, Ag^+, or some combination, with $NaBH_4$ in the presence of the surfactant in toluene solutions.[38] These surfactant-coated nanoparticles were subsequently drop-cast deposited between microfabricated electrodes for vapor[38,55] and gas[55] sensing applications.

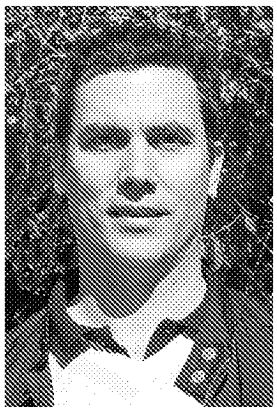

Francisco J. Ibañez obtained his Bachelor degree in Chemical Engineering at Universidad Tecnológica Nacional (UTN), in Mendoza, Argentina. He performed environmental studies in Japan at the University of Hiroshima in 2000. In 2001, He joined Prof. Zamborini's group at the University of Louisville (Kentucky, USA) where he obtained a PhD in Chemistry. He is currently a Professor of Materials Engineering at the Universidad Nacional de La Plata (UNLP) and Assistant Researcher at the Instituto de Investigaciones Fisicoquímicas Teóricas y Aplicadas (INIFTA-UNLP-CONICET), La Plata, Buenos Aires, Argentina in the group of Dr. Roberto C. Salvarezza. His research focuses on electronic and optical properties of organic-modified nanoparticles and their use in sensing and energy-storage applications.

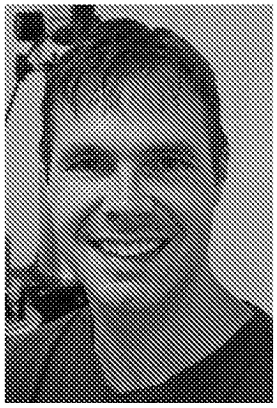

Francis P. Zamborini graduated from Texas A&M University in 1998 with a PhD in Chemistry, focusing on corrosion passivation and lithography with organomercaptan SAMs with Richard M. Crooks. He then conducted research on the synthesis, assembly, and electron-transport properties of gold monolayer-protected clusters under Royce W. Murray at the University of North Carolina at Chapel Hill as a postdoctoral research associate until 2001, when he joined the faculty at the University of Louisville. He is currently a professor in the Analytical Division of the Department of Chemistry. His research focuses on the controlled synthesis and assembly of metallic nanostructures and their electronic, electrochemical, and optical properties for applications in chemical and biochemical sensing.

2.3. Monolayer-Protected Clusters (MPCs)

MPCs are most often synthesized by reducing a metal ion precursor in the presence of organomercaptans or organoamines, which serve as stabilizing ligands, in a one-phase or two-phase solvent system. As the metal salt is reduced to the zero-valent metallic form, nanoparticles form by nucleation and growth while the organic ligands adsorb onto the surface of the nanoparticles to form a single self-assembled monolayer (SAM) coating. The SAM passivates the nanoparticle surface, prevents nanoparticle aggregation, and controls

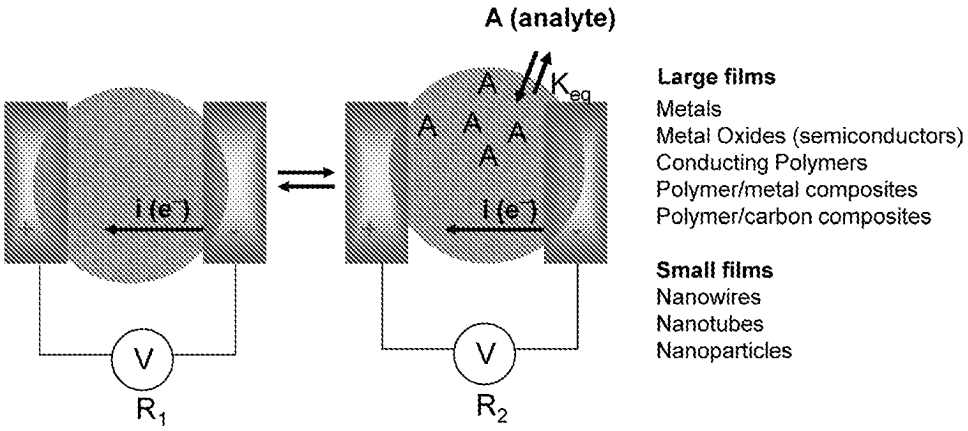

Figure 1. Schematic representation of a chemiresistive film placed in between two metal electrodes subjected to a potential (V) where film resistance R_1 changes to R_2 upon interaction between film and analyte (A) of interest.

Table 1. Summary of the organic-modified metal and alloy nanoparticles used for chemiresistive sensing. Note: 2-propanol = IPA, methanol = MeOH, ethanol = EtOH, benzene = Bz, hexane = Hx, toluene = Tol, tetrahydrofuran = THF, dichloromethane = Cl_2CH_4, 11-mercaptoundecanoic acid = MUA, 6-mercaptohexadecanoic acid = MHA, 16-mercaptohexadecanoic acid = MHDA.

Metal composition	NP size + STD [nm]	Modifier	Linker	Film deposition method	Sensing environment	Analytes detected	LOD	Current increase (↑) decrease (↓)	Ref.
Au	NR	octanethiol (C8S)	—	airbrush	air	water, IPA, tetrachloroethylene, Tol	2.7 ppm (Tol)	↑ and ↓	[27]
Au	2.9–6.0	hexanethiol C6S-X with X = OH, NH_2, CH_3, COOH	—	spin-coating	air	MeOH, IPA, Hx, pentane, Tol, acetic acid	20-10 ppm (EtOH)	↑	[28,86]
Au	2.0 ± 0.8	$CH_3(OCH_2CH_2)_nSH$ n = 2,3,4	—	airbrush	air	water, IPA, Tol	NR	—	[29]
Au	3.0–5.0	n-(3-thienyl)alkanethiols n = 2,6,12	—	spin-coating	air	EtOH, chloroform, Hx, Tol	NR	—	[30]
Au	4.3 ± 0.9	C8S; $PtCl_2$(olefin)-pyridine) +C8S	—	airbrush	air	EtOH, acetone, 2-butanone, isooctane, trichloroethylene, 1-4 dioxane, Tol, perchloroethylene, n-butyl acetate, chlorobenzene, m-xylene, styrene, ethylene, 1-octane, 1.3-butadiene	≈5.5 ppb (styrene)	↓	[31]
Au	3.0–4.0	C8S; octanetrithiol ($C8S_3$)	—	inkjet-printing	NR	Tol, EtOH, dichloroethane, MeOH, and acetone	300 ppm (Tol)	↓	[32]
Au	4.3 ± 0.9	C8S	—	spray-coating	N_2	28 different vapor analytes	0.0079 ppm (n-decane)	↓	[33]
Au	3.9–4.5	1-octanethiol (C8); 1-mercapto-6-phenoxyhexane (OPH); 7-hydroxy-7,7-bis(trifluoromethyl)-heptane-1-thiol (HFA), or mercapto-diphenylacetylene (DPA)	—	micro-dispensing	NR	n-propanol 2-butanone	NR	↓	[34]
Pt	17 ± 0.5	oleylamine (ODA),11-mercaptoundecanol, MUA, and benzylmercaptan	—	drop-casting	dry and humid air	Hx, octane, decane, ethyl Bz, EtOH, and water	40 ppm (octane)	↓	[35]
Au	NR	chlorobenzenemethanethiol (CBMT), C8S	—	immersion	air	IPA, acetone, cyclohexane	185 ppm (Tol)	↓	[36]
Au	6.0–7.0	$C12NH_2$	—	drop-casting	air	water, acetone, Tol, methanethiol, propanethiol, octanethiol, and thiols diluted in N_2	1.5 ppm (methanethiol)	↑	[37]
Au; AuAg	4.1 ± 0.8	tetraoctylammonium bromide (TOABr)	—	drop-casting	air	MeOH, EtOH, IPA, Tol, acetone	2.0 ppm (EtOH)	↑	[38]
Au	5.2 ± 0.3 1.9 ± 0.7	C12S	(1,9 nonanedithiol, NDT), (MUA)	place-exchange cross-linking precipitation	air	EtOH, Hx, Tol	NR	—	[39]
Au	2.0 ± 0.7	C12S	X–$(CH_2)_n$–X; X = COOH,HS; n = 6,9,12,16	place-exchange cross-linking precipitation	air	Bz, Hx, Tol	NR	—	[40]
AuAg	2.0–3.0 (±0.5)								
Au	≈1.6	C6S	hexanedithiol	microcontact printing	N_2	IPA, Tol	NR	—	[41]

Metal composition	NP size + STD [nm]	Modifier	Linker	Film deposition method	Sensing environment	Analytes detected	LOD	Current increase (↑) decrease (↓)	Ref.
Au	NR	$C12NH_2$	[1,12-dodecanedithiol]; [(4)-staffane-3,3‴-dithiol]; [4,4′-terphenyldithiol]	layer-by-layer	air	Tol, 1-propanol, 4-methyl-2-pentanone, water	NR	—	[42]
Au	≈1.1	[poly(ethylene glycol) thiol (HSPEG)]; [phenyl ethane thiol (-SC_2Ph)]	octanedithiol and decanedithiol	liquid-phase cross-linking	air	Hx, EtOH, CO_2	NR	—	[21]
Au	4.0 ± 1.2	$C12NH_2$	dodecanedithiol	layer-by-layer	air	Tol, 4-methyl-2-pentanone, water, 1-propanol	NR	—	[43]
Au	NR	C_nS, n = 4,6,8,10,12, MUA, MHA, MHDA	$HS(CH_2)_nCO_2H$, n = 5,10,15	drop-casting	N_2	EtOH	NR	—	[44]
Au; Ag; Pd	1.0–3.0	C6S; MUA	Carboxylate-M^{n+}-carboxylate, n = Cu^{2+}, Zn^{2+}, Ag^{+}, or methyl viologen	layer-by-layer	air	EtOH	NR	—	[45]
Au	≈4.0	$C12NH_2$	[disulfide polyphenylene]; [poly(amidoamine)]; [poly(propylene imine)]	layer-by-layer	air	water, 1-propanol, Tol	NR	—	[46]
Pt, Au	3.0 ± 0.8	$C12NH_2$	1,9 nonanedithiol	layer-by-layer	air	water, NH_3, CO, Tol, tetrachloroethylene	100 ppb (NH_3)	↓	[47]
Au	3.0	1H, 1H, 2H, 2H Perfluorodecanthiol (PFDT)	—	drop-casting	N_2	hexafluorobenzene, MeOH, Hx, chloroform, Tol, water	NR	↑	[48]
Au	NR	C_nS, n = 4-11	—	drop-casting	NR	*n*-hexane, *n*-heptane, *n*-octane, iso-octane, cyclohexane,Tol, ethyl acetate, MeOH, EtOH, IPA 1-butanol	NR	↑ and ↓	[49]
Au	NR	C8S	1,6 Hexanedithiol and 1,4 benzenedimethanethiol	place-exchange cross-linking precipitation	N_2	water vapor, Tol, EtOH, ethylacetate, IPA, and acetonitrile	4 ppm (Tol)	↓	[50]
Pd	1.7–113.8	λ-DNA	—	drop-casting	air	H_2	1000 ppm	↑	[51]
Au	NR	C6S; C10S; 4-methylbenzethiol	—	Langmuir–Schaeffer	air	Tol, NO_2	0.5 ppm (NO_2)	↑ and ↓	[52]
Au	3.2–11.8	C6S	—	immobilized on SAM-modified surface	air	Hx, Tol, ethyl ether, THF, $CHCl_3$, CH_2Cl_2, acetone	NR	—	[53]
Pd; PdAg PdAu	≈3.0	C6S; $C8NH_2$; $C12NH_2$; $C16NH_2$; TOABr, mix-monolayer (C6S+$C8NH_2$)	—	drop-casting	N_2 and air	H_2	800 ppm	↑	[55,75]
Au	≈6.0	C6S; [4-mercaptophenol]; [6, Hydroxyexanethiol]	—	inkjet-printing	liquid	EtOH, Cl_2CH_4, Tol, octane	0.1 ppm (Tol)	↓	[54]
Au	≈3.0	C8S	—	drop-casting	liquid	C8S and Galvinol	pH sensitive	—	[56]
Au	≈6.0	polymethtylene	—	immobilized on a redox-gate	liquid	bypiridinium	oxidation/reduction	—	[57]
Au	≈13	oligonucleotides	—	Immobilized on a oligonucleotide-strands	liquid	DNA	500 femtomolar	—	[58]
Au	13.0 ± 20	3-mercaptopropionic acid	Zn^{4+}	immobilized on a peptide nucleic acid	liquid	DNA	50 femtomolar	—	[59]

the nanoparticle solubility. The study of SAMs on various planar and nanostructured metal surfaces has been crucial to the understanding of the physical and chemical properties of these interesting materials and their interactions.[64] For instance, nanoparticle size depends on the SAM molecule to metal ion mole ratio during the synthesis. As the ratio increases, the nanoparticle size decreases and is in the general range of 2 to 5 nm in diameter for Au nanoparticles protected with alkanethiolates.[65] Some examples of organomercaptan ligands used in nanoparticle synthesis include the commonly used hexanethiol-coated (C6S) Au MPCs,[66] octanethiol-coated (C8S) Au MPCs,[27] a mixture of alkanethiol and ω-carboxylate alkanethiol (i.e., 11-mercapto-undecanoic acid, MUA) MPCs,[44] and some examples of organoamine ligands include dodecylamine-coated ($C12NH_2$),[37,67] and octylamine-coated ($C8NH_2$) Pd and PdAg alloy MPCs,[55] and dodecylamine-coated ($C12NH_2$) Pt,[47] Au,[47] and PdAu[55] alloy MPCs. Alternatively, monolayer-protected nanoparticles can be synthesized by reducing the metal ion precursor with weakly coordinated ligands, such as citrate ions or surfactants (vide supra), which are then later exchanged with stronger organomercaptan ligands to form MPCs. There are also a few methods used to alter the functionalization of MPCs by post-synthetic chemical treatments. This includes place exchange reactions, where the original monolayer is completely or partially exchanged with an incoming new ligand either in the liquid phase or the vapor phase.[68] Coupling reactions[69] with reactive groups on the MPCs also lead to more diverse functionalization. The thermal treatment of MPCs in solution has been utilized after synthesis to increase the particle size and decrease size dispersity.[70]

3. Device Fabrication

3.1. Electrode Devices

Electrode devices are usually microfabricated in a cleanroom facility following photolithography, sputtering, and lift-off procedures. Microelectrodes are sputtered or evaporated over an insulating layer (i.e., Si/SiO_x) and, less commonly, over an insulating flexible polymer[71] with a pair of Au electrodes or interdigitated array (IDA) of electrodes separated by micro- or nanometer distances.[41,58] The IDA consists of several (10–20, usually) interdigitated Au fingers separated by a few to tens of micrometers.[27,44] A conductive STM tip and sample has also been used for studies of electron tunneling at a junction containing individual nanoparticles.[53]

3.2. Nanoparticle Deposition/Assembly

To complete device fabrication, the organic-modified metal nanoparticles must be assembled or deposited across two electrodes by some method in order for their electronic properties to be measured. The strategy varies, depending on the type of metal nanoparticle synthesized. Electrostatically-stabilized metal nanoparticles, such as citrate capped nanoparticles, are usually assembled through bifunctional cross-linkers, such as dithiols,[72] or electrostatically with polyelectrolytes.[73] This requires sequential dipping of the electrodes into alternating solutions of the metal nanoparticles and the cross-linker or polyelectrolyte.[74] Surfactant- or polymer-coated nanoparticles could be water-soluble or soluble in organic solvents and deposited across electrodes by drop-cast deposition or layer-by-layer assembly.[38] Nanoparticles coated with biological molecules, such as DNA or proteins, may be deposited on surfaces through specific biological interactions.[58]

MPCs are usually soluble in organic solvents, depending on the polarity of the SAM, and therefore deposited across electrodes (often IDAs) by drop-coating,[75] airbrushing,[27,28] and spin coating.[28,30,36,76] Layer-by-layer deposition is also possible as has been demonstrated with dithiols,[77] dendrimers,[46] and metal ion–carboxylate linkages.[44,45] Zhong and co-workers developed a cross-linking precipitation method[93] and studied the implications of linked nanoparticles[71] where organic soluble MPCs become insoluble by adding ligands that cross-link the MPCs through dithiol or hydrogen bonding interactions and deposit directly across the electrodes from solution. Recently, MPCs have also been deposited by microcontact printing,[41] lithography techniques,[78] inkjet-printing,[79] and microdispensing.[34]

Figure 2 shows the deposition of a film of nanoparticles by drop-casting, dipping cycles in a layer-by-layer fashion, microfabrication, and microcontact printing approaches. Figure 2A shows optical images of microelectrodes before and after drop-cast deposition of a film of $C8NH_2$ Pd MPCs.[55] Figure 2B shows Au nanoparticles assembled between two Pt electrodes by immersion of the electrodes in an alkanedithiol solution followed by the nanoparticle solution and repeating the procedure to form films in a layer-by-layer fashion.[76] Figure 2C shows microfilms of Au MPCs obtained by microfabrication techniques.[78] Our group also combined microcontact printing with vapor phase dithiol cross-linking to prepare highly stable microscale films of Au MPCs that respond reversibly to volatile organic compounds (VOCs)[41] and H_2 gas and that were connected by Ag paint[75] in the top and bottom images of Figure 2D, respectively.

4. Electronic Properties of Chemically Modified Metal Nanoparticles

4.1. 3D Solid-State Films of Metal Nanoparticles

The conductivity of solid-state 3D films of organic modified metal nanoparticles, mainly discussed in the literature for MPCs, has been described as an activated core-to-core electron hopping mechanism by the following equation:

$$\sigma_{EL} = \sigma_0 \exp\left[-\beta_d \delta_{edge}\right] \exp\left[-E_A/RT\right] \quad (1)$$

Here, σ_{EL} is electronic conductivity (Ω^{-1} cm^{-1}), σ_0 is a pre-exponential constant, δ_{edge} the core edge-to-edge distance, β_d is the electron tunneling coefficient (Å^{-1}), E_A is the activation

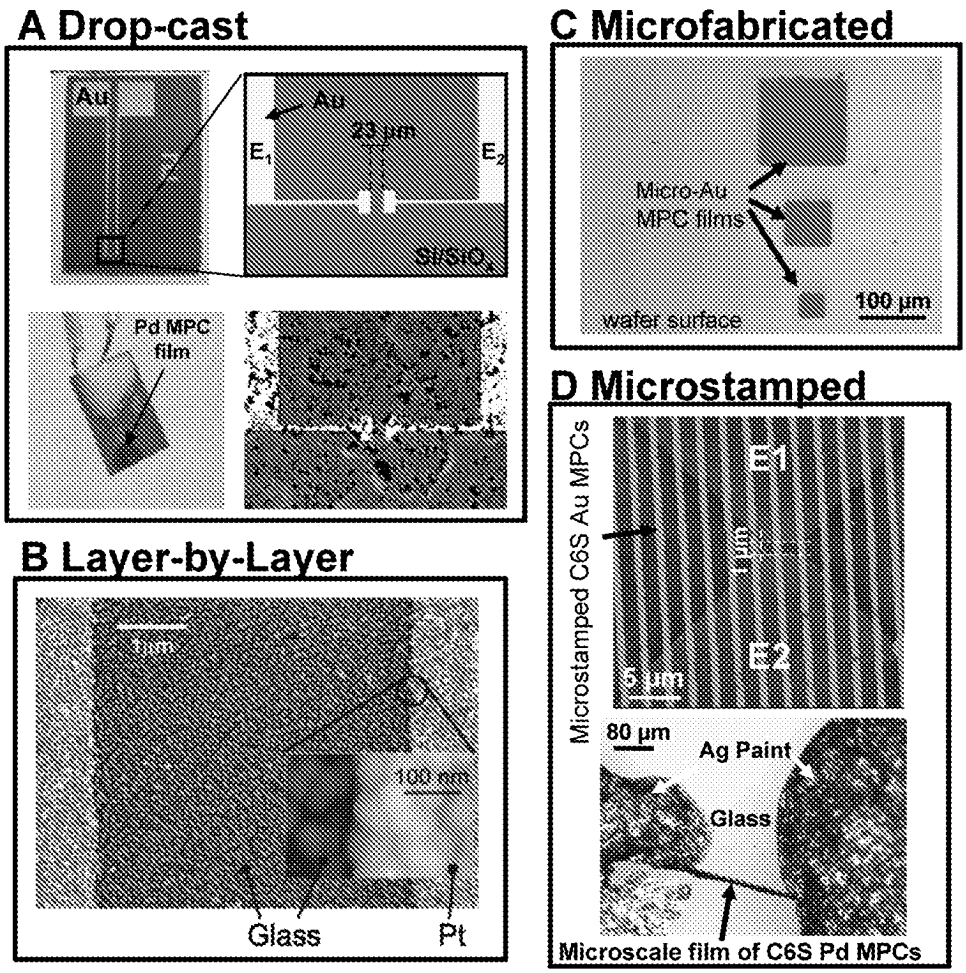

Figure 2. A) Optical image of a 23 μm gap electrode before and after drop-casting $C8NH_2$ Pd MPCs; B) SEM and close-up image of an Au nanoparticle film formed by repeated dipping cycles in alkanedithiol and Au nanoparticles solution; C) SEM image of microfabricated Au nanoparticle films of various dimensions, and D) AFM image of microstamped lines comprised of C6S Au MPCs across two Au electrodes separated by 1 μm and an optical image showing Ag paint contacting a microwire comprised of C6S Pd MPCs. Reproduced with permission.[A][75][B][76][C][78][D][75]

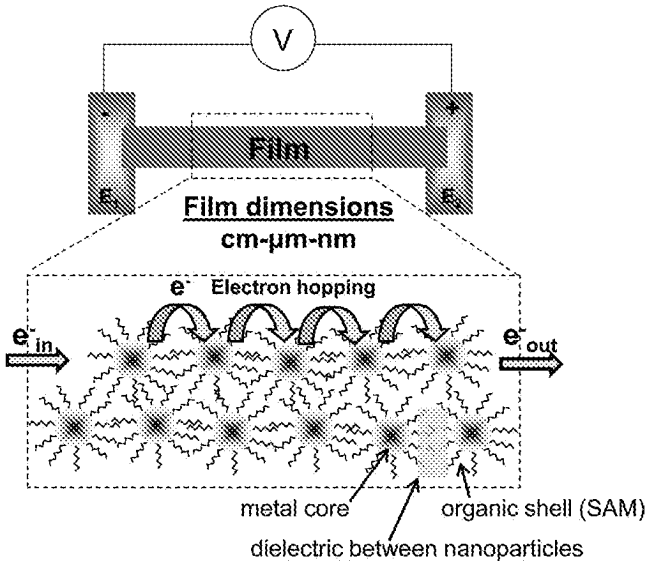

Figure 3. Schematic representation of a chemiresistive film of various dimensions comprised of metal monolayer-protected clusters (MPCs) separated by interdigitated SAM molecules. Electron hopping occurs from core to core when a voltage (V) is applied.

energy (kJ mol^{-1}), R the gas constant, and T the temperature in Kelvin.

The cartoon in **Figure 3** shows MPCs separated by interdigitated self-assembled monolayer (SAM) molecules through which electron hopping occurs. The first term in Equation 1 shows that σ_{EL} is exponentially dependent on the nanoparticle-nanoparticle edge-to-edge distance (δ_{edge}) and the tunneling coefficient (β_d). The value of δ_{edge} depends on the number of carbons in the alkyl chain of the SAM (or its thickness), which determines the distance between the cores. The tunneling coefficient (β_d), usually referred to as an attenuation factor describing the exponential decay in electron transfer as the distance between the nanoparticle cores increases, depends on the structure and molecular composition of the SAM. For example, aromatic groups have a smaller β_d compared to alkane chains due to electron delocalization in aromatic rings. The dielectric constant of the SAM, ε_s, (vide infra) may also affect β_d. For example, an Au nanoparticle coated with similar chainlength SAMs with different end groups, such as dodecanethiol versus mercaptoundecanol, might have different β_d values.

The second exponential term in Equation 1 relates conductivity to the temperature and the energy of activation. For continuous metal films, σ_{EL} decreases as temperature increases. In discontinuous films, such as films of MPCs or ultrathin films comprised of 2–8 nm diameter metal islands (granular films), the conductivity increases with increasing temperature. The conductivity is exponentially dependent on T^{-1} or $T^{-1/2}$ in the Arrhenius and granular models,[80] respectively. Terrill et al. compared the Arrhenius and granular models for conductivity of films of Au MPCs, finding that ln(conductivity) was linearly dependent upon both T^{-1} and $T^{-1/2}$ within experimental error.[81] From the slope of the Arrhenius or granular model plots, one can measure the activation energy (E_A), which is equivalent to the energy required to transfer an electron between neutral cores to generate a positively and negatively charged nanoparticle pair (also termed charging energy). This activation energy depends on the dielectric of the surrounding medium, energy of an electron, and radius of the particle as discussed by both Sheng et al.[82] and Terrill et al.[81] as follows:

$$E_A \approx N_A e^2 \delta_{edge} / \varepsilon_S \varepsilon_0 R_{core} \left(R_{core} + \delta_{edge}\right) \quad (2)$$

where N_A is Avogadro's number, e the electronic charge, δ_{edge} the core edge-to-edge separation, 'R_{core}' the radius of the metal nanoparticle, 'ε_s' the static dielectric constant of the intervening matrix, and 'ε_0' the permittivity of free space.

Equation 2 shows that E_A is inversely proportional to the dielectric constant of the medium (ε_s). Since σ_{EL} has an inverse exponential dependence on E_A, an increase in ε_s will lead to a decrease in E_A and a corresponding exponential increase in σ_{EL}. In general, σ_{EL} from Equation 1 will change if an analyte of interest partitioning into the film of nanoparticles causes a change in δ_{edge} through film swelling or E_A and β_d by significantly altering the dielectric properties surrounding the monolayer. For sensing experiments at constant T, a change in all three variables will affect the conductivity and it is often not known which variable is the dominant factor. A more dramatic change from electron hopping to metallic conductivity occurs if the discontinuous film changes into a continuous film with a fully conductive pathway beyond the percolation threshold.[83,96]

4.2. Individual Nanoparticles

Most previous knowledge of the electronic properties of individual metal nanoparticles derives from scanning tunneling microscopy (STM) experiments, where one measures the tunneling current (I_{tun}) between a sharp metallic STM tip and a conductive substrate through an individual metal nanoparticle as a function of the bias voltage (V_{bias}) applied between the tip and substrate. The relationship between tunneling current and V_{bias} in STM is as follows,[84]

$$I_{tun} = (\text{const})\, V_{bias} \exp(-2\beta d) = V/R_{tun} \quad (3)$$

where d is the distance between the STM tip and conductive surface, β is the electron tunneling decay constant (≈1 Å^{-1}), and R_{tun} is the effective resistance of the tunneling gap,

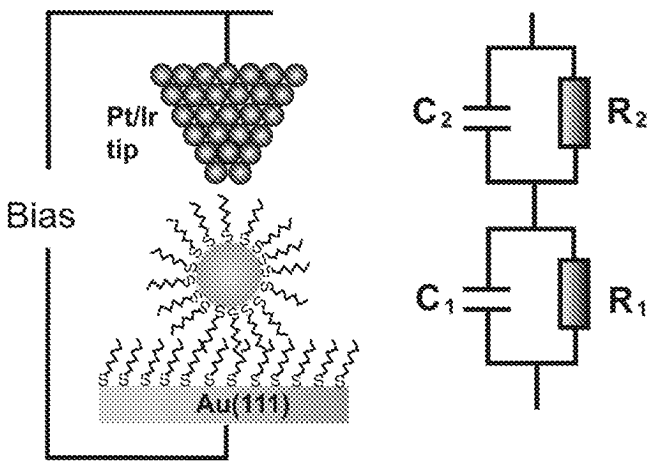

Figure 4. Schematic representation of electron tunneling between an STM tip and a SAM-modified Au substrate through a single MPC. The circuit represents the interaction between tip–MPC and the MPC–substrate with capacitors (C_1 and C_2) and resistors (R_1 and R_2) in series. Reproduced with permission.[53]

typically 10^9–10^{11} ohms.[84] This equation shows the well-known exponential relationship between I_{tun} and tip–sample distance, which is similar to the exponential relationship between conductivity and nanoparticle edge-to-edge distance for electron hopping between metal nanoparticles. Clearly, a small change in d leads to a dramatic change in I_{tun} (about 1 order of magnitude change with a 1 Å change in distance). **Figure 4** shows a schematic diagram of an experiment incorporating a Pt/Ir STM tip over a conductive substrate with a single MPC on the surface placed between the tip and the substrate.[53] There is a barrier to electron transport at the tip–MPC and MPC–substrate junctions, which depends on the capacitance and resistance of these junctions as depicted in Figure 4. The energy required to charge a single nanoparticle by one electron is given by:

$$E_c \simeq e^2/2C \quad (4)$$

where e is the electron charge and C is the capacitance of the nanoparticle. In order to observe single electron transfer events at individual nanoparticles, E_c must be much greater than the available thermal energy kT. The capacitance of a nanoparticle depends on the radius and dielectric surrounding the nanoparticle according to:

$$C = 4\pi\varepsilon_S r \quad (5)$$

where ε_s is the static dielectric of the medium and r the radius of the nanoparticle. Considering Equations 3 and 4, E_c increases with decreasing nanoparticle size. When the nanoparticle size is small enough that E_c is much greater than kT, Coulomb blockade or staircase behavior may occur and be observed in an STM experiment.[53] The change in voltage (Coulomb gap or step) corresponding to the single electron tunneling event as determined from a current–voltage (I–V) curve is related to electron charge (e) and capacitance $E_c = e^2/2C$. This can be used to measure the nanoparticle capacitance experimentally.

For a constant size nanoparticle, if an analyte binding event changes the dielectric (ε_s), then the capacitance will change proportionally and the Coulomb gap or step observed in the I–V curve will change. Since scanning tunneling spectroscopy (STS) experiments are very sensitive to the environment of the nanoparticle, some groups have used organic-modified metal nanoparticles as chemical gates and studied single electron transport (SET) at different pH,[56] through redox molecules,[57] and at single MPCs of different size in the presence of various vapor analytes.[53] These examples will be described in more detail later in this review.

5. Partitioning and Response of Chemiresistive Sensors

All sensors consist of an analyte delivery system, sensitive coating material, and a transduction element that converts a chemical or physical interaction between the analyte and sensitive coating into a measurable electronic signal. When analyzing molecules in the vapor phase, the analyte is usually transported to the sensing device by an inert carrier gas, such as N_2, or Ar, or is detected in air under ambient conditions. In a chemiresistive sensor, the vapor phase analytes partition into the sensitive film and a direct change in the resistance of the film provides the signal for quantifying the vapor concentration of the analyte. The concentration of the analyte in the sensitive film (C_f) is related to the concentration of the analyte in the vapor phase (C_v) at equilibrium by the partition coefficient (K_d) as shown in the following equation:[85]

$$K_d = C_f/C_v \quad (6)$$

The sensor response (R_s) is usually assumed to be directly related to C_f, which is directly related to K_dC_v as follows:

$$R_S = f(K_dC_V) \quad (7)$$

K_d depends on the relative affinity of the vapor phase molecules for the film versus the vapor phase. The same rules observed for separation methods, such as gas chromatography, also apply for the film coatings of the vapor sensors. For example, a nonpolar molecule will have a larger affinity for a nonpolar film and vice versa. In addition, analyte molecules with lower vapor pressure will generally favor the film, or the condensed phase. If there is a specific chemical interaction between the vapor molecule and the film, other than just similar polarity, then a very large K_d may result. Many researchers model the response of the sensor as a function of the vapor phase concentration according to the Langmuir adsorption isotherm model as follows,[77]

$$R_{s,max}/R_S = 1 + 1/K_dC_V \quad (8)$$

where $R_{s,max}$ is the maximum response of the sensor at saturation and R_s is the response of the sensor at the particular vapor concentration C_v. By plotting $R_{s,max}/R_s$ versus $1/C_v$, one can obtain K_d from 1/slope of the linear plot if the vapor adsorption to the film follows this model. For liquid phase analytes, the situation is similar except that the analyte molecules partition between the liquid phase medium and the solid-phase chemically sensitive film.

In the next three sections of the review, we describe the use of chemically modified metal nanoparticles as the sensitive coating in chemiresistive sensors for organic vapor molecules (Section 6), gases (Section 7), and liquid-phase molecules (Section 8).

6. Chemiresistive Sensing of Vapor-Phase Molecules

6.1. Drop-Cast 3D Films

6.1.1. Drop-Cast Films of Organomercaptan-Coated Au Nanoparticles

Effect of Functionality: Wohltjen and Snow were the first to report on the use of Au MPCs for chemiresistive sensing of VOCs. They prepared a drop-cast film of octanethiolate (C8S)-protected Au MPCs for chemiresistive sensing of polar and nonpolar vapor-phase analytes, including water, 2-propanol, tetrachloroethylene, and toluene.[27] In their studies, they synthesized and purified the C8S Au MPCs, dissolved them in toluene, and drop-coated a solid-state film of the C8S Au MPCs across an interdigitated array (IDA) of electrodes for chemiresistive measurements. **Figure 5**A shows the relative conductance change ($\Delta S/S$) versus the vapor pressure of the different vapor analytes. The relation demonstrates a drastic current decrease of the film in the presence of toluene, no change in water, and a slight current increase for the film in the presence of 1-propanol. The authors concluded that there were two electron-transport mechanisms occurring at the film: electron tunneling between metal cores (≈2 nm spacing) and hopping along the alkanethiol chain. The large film response upon toluene absorption was attributed to a dominant swelling mechanism, which locally perturbed the electron transport between cores by increasing the interparticle distance. They suggested that adding specific functional groups to the organic layer would allow selectivity and sensitivity for a wide range of vapor analytes.

In a later study, Evans and co-workers prepared drop-coated films of Au MPCs protected with S–C_6H_4–X, where X = –OH, –COOH, $–NH_2$, and $–CH_3$, for sensing methanol (MeOH), ethanol (EtOH), 2-propanol, hexane, pentane, toluene, chloroform, and acetic acid.[28,86] Films containing MPCs with X = CH_3 displayed the largest response to nonpolar analytes, such as pentane and hexane, while those coated with polar X groups were more sensitive towards OH-containing vapors. They suggested that this trend could be understood in terms of solubility between the analyte and the protecting ligand. Following their report,[28] they introduced two MPC films that were more stable in solution as compared to –COOH- and $–NH_2$-terminated nanoparticles. Figure 5B shows films comprised of 4-mercaptophenol (X = –OH) and 4-methylbenzenethiol (X = $–CH_3$)-functionalized Au MPCs used for sensing nonpolar dichloromethane

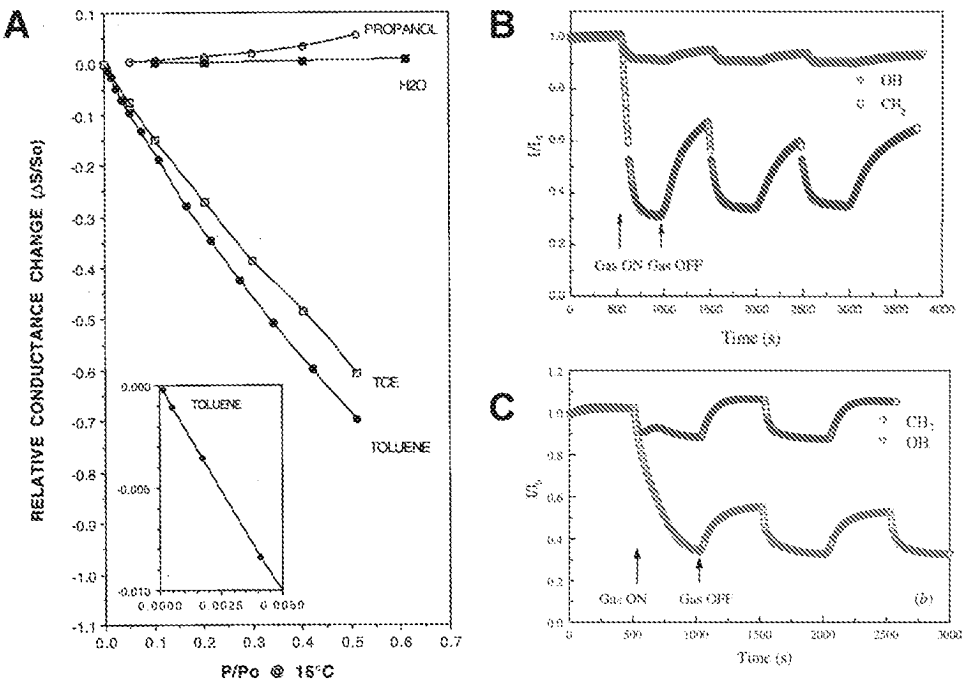

Figure 5. A) Vapor response isotherms of the C8S Au MPC film exposed to propanol, water, tetrachlorethylene (TCE), and toluene. B,C) Chemiresistive response for S–C_6H_4–X-coated Au MPC films with X = –OH or –CH_3, towards dichloromethane (DCM) and methanol vapor, respectively. Reproduced with permission.[A][27][B,C][28]

(DCM) and polar MeOH analyte vapors shown in Figure 5B and C, respectively. It is noticeable from the response profiles that films with OH-containing groups were more selective to a 91 ppth MeOH vapor indicated by a drop in film current of approximately 70% as compared to nonpolar analytes, which displayed only a 20% current change in the presence of the same film. Accordingly, films comprised of CH_3-containing groups were more responsive to DCM. Interestingly, an increase in conductivity occurred for a film of OH-functionalized Au MPCs in the presence of lower MeOH concentration. The authors explained the current response based on the electron hopping Equation 1, where the current increased at low concentrations of MeOH due to an increase in the permittivity of the film (ε_s) as the MeOH molecules partition into the interstitial pores between MPCs in the film, and the current decreased at high vapor concentration due to film swelling upon a greater amount of MeOH in the film, which led to an increase in the edge-to-edge MPC distance (δ_{edge}) that dominated over the permittivity increase. The authors determined that the MPC separation and permittivity of the medium depends on the analyte partial vapor pressure.

Foos et al. exchanged conventional C6S Au MPCs with ethylene oxide oligomers $CH_3(OCH_2CH_2)_nSH$ of specific lengths (n = 2, 3, and 4) and studied their solubility, conductivity, and chemiresistive response to VOCs.[29] They observed that when n = 2, the nanoparticles were water-soluble while they were water insoluble when n > 2. All of the film conductivities were roughly one order of magnitude larger than that of alkanethiol-coated Au MPCs of similar length. In the presence of toluene, in all cases the film of ethylene oxide MPCs exhibited a decrease in current, but it was more pronounced for shorter organic chains (n = 2). In the presence of 2-propanol and water, these films exhibited a weaker response and sometimes an increase in current, similar to that observed for C8S Au MPCs[27] and small aromatic thiol-coated Au MPCs.[86] In general, the film with low content of oligomer units responded best to toluene. As the oligomer units in the nanoparticle increase, the reponse to nonpolar vapors such as toluene dimished, suggesting a mismatch in polarity between the film and the vapor analyte.

Whitten and co-workers studied the electrical response of films of thiophene-terminated alkanethiol MPCs with three different chainlengths upon exposure to vapors of toluene, EtOH, chloroform, and hexane over a concentration range of 1000 to 200 000 ppm.[30] The chemiresistive response trend followed as toluene > chloroform > hexane > EtOH, which is consistent with the fact that the film is nonpolar and the response is greatest for nonpolar analytes. The nonpolar analytes partition more strongly into the film relative to more polar analytes, leading to a greater degree of film swelling and larger sensor response by a decrease in the conductivity. At large EtOH concentration, researchers observed an increase in current, which they concluded was due to an increase in the dielectric constant (or permittivity) in the medium around the Au MPCs as discussed earlier.[27,86] A more recent study from the same group revealed that perfluorinated dodecanthiol (PFDT)-coated Au MPC films exhibit a decrease in resistance in the presence of polar and nonpolar vapor analytes.[48] The authors observed relatively large spacing between Au cores (3.0 nm) suggesting that the tails of the PFDT chain might be touching each other (not interdigitated). This conformational film structure and separation between particles led the authors to speculate about the anomalous sensing behavior. They suggested that dielectric effects may dominate over swelling based on the observed

increase in conductivity of the film for all vapors tested. The authors suggest that based on the film structure, islands of nanoparticles in the presence of the vapor may approach one another or separate from each other, resulting in the formation of more conductive pathways as previously discussed by Vossmeyer and co-workers.[77] This report shows for the first time that a 3D film comprised of MPCs responded with an increase in conductivity in the presence of polar and nonpolar vapors.

Rowe et al. prepared films of C8S Au MPCs alone and C8S Au MPCs mixed with $PtCl_2$(olefin)–(pyridine) square planar coordination complex for the detection of various vapors and olefins.[87] A comparison between the C8S Au MPCs with the mixed film (C8S + Pt complex) showed that the complex-containing olefin film was more selective and sensitive towards olefin gases. The C8S film by itself displayed an increase in resistance in the presence of all the vapor analytes tested while the Pt complex film showed a decrease in resistance. The complex-containing olefin coordinated with the target olefin and readily returned to the original coordinated-square planar geometry after analyte dissociation. As the olefin analyte binds to the Pt complex a decrease in resistance of the composite film was observed and attributed to the formation of low resistance pathways caused by the analyte which somehow competes with the increase in resistance usually observed in the C8S MPC films alone. To prove analyte loading on the film, the researchers monitored mass changes with a thickness shear mode resonator (TSMR). They concluded that the LOD for the film of Au MPCs with the Pt-olefin complex is several orders of magnitude lower than the C8S Au MPCs film alone particularly for the olefin gases ethylene and 1,3-butadiene. However, the composite film responded and recovered slowly and deteriorated over time, which limits their use in GC applications.

Kim et al. prepared films of Au MPCs coated with mixed ligands of chlorobenzenemethanethiol (CBMT) and n-octanethiol for chemiresistive sensing of 1-propanol, acetone, and cyclohexane.[36] The results showed that mixed monolayer MPCs exchanged with higher octanethiol content (≈80% molar ratio used in the ligand replacement reaction) were more responsive to cyclohexane and 1-propanol, which is surprising in the latter case due to the higher polarity. On the other hand, films of MPCs with lower amounts of octanethiol (50% molar ratio) were more selective towards acetone.

Cai et al. prepared films of C8S Au MPCs and 2-phenylethanethiol and assembled them onto an IDA of electrodes for chemiresistive sensing and gas chromatography (GC) quantification of 11 vapors.[31] The analytical device consisted of a sensor array with four different IDA dimensions placed on top of a preconcentrator capable of thermally desorbing the gases for GC separation and quantification. The response to vapors was linear, reproducible, and very sensitive with an LOD ranging from 0.1 to 24 ppm. When analyzed in the preconcentrator for GC applications, the response lowered to 700 parts per trillion. This was the first report that elegantly showed a combination of chemiresistive response patterns and GC retention times, which greatly improves vapor recognition as compared to the sensor array alone.

Recently, Peng et al. prepared nine different functionalized Au MPCs and drop-casted them onto an IDA of electrodes for chemiresistive sensing of exhaled breath from healthy and unhealthy (lung cancer) patients.[88] The researchers were able to identify 42 different exhaled VOCs which were used as lung cancer biomarkers. In their work, they suggested that acetaldehyde and formaldehyde VOCs can be associated with breast and lung cancer, respectively. They demonstrated that a combination of an array chemiresistor coupled with GC/MS and the use of principal component analysis (PCA) can discriminate between healthy and unhealthy patients in humid atmosphere and without the need of preconcentrators. Following their report, the same group was able to discriminate between healthy and unhealthy patients from a pool of 177 volunteers. They used an array of nanoparticles and GC for the measure of VOCs and mass, respectively, and were able to differentiate between breast, prostate, and colorectal cancer.[89]

Garg et al. prepared trithiol-capped Au MPCs and deposited them by inkjet-printing on a spiral Au IDA of electrodes for chemiresistive sensing of various analytes including Tol, EtOH, dichloroethane, MeOH, and acetone.[32] They compared stability of the trithiol-protected Au MPC films with the conventional monothiol C8S Au MPCs. They observed that after six months the sensitivity of the trithiol-capped MPCs film was reduced by ≈10% while a conventional monothiol film decreased by ≈47%, indicating that multiple thiols chemisorbed on the Au nanoparticles are relatively more resistant to oxidation.

Effect of Chainlength: Through chemical synthesis, it is possible to tailor the length of the monolayer surrounding the MPCs and therefore control the electronic properties of the film. Ahn et al. prepared films of 12-(3-thienyl)-dodecanethiol-, 6-(3-thienyl)hexanethiol-, and 2-(3-thienyl)-ethanethiol-protected Au MPCs and exposed them to vapors of toluene, EtOH, chloroform, and hexane.[30] Films containing the greatest number of methylene units responded greater to both polar and nonpolar vapors in a range from 1000 to 5000 ppm. Based on these results, the authors concluded that while films of MPCs coated with thiols with a larger number of methylene units displayed lower conductivity, they provided more absorption sites for the film to interact with the analyte and swell, and therefore improved sensitivity.[30] These films have a larger K_d, which leads to a larger response according to Equation 7 and 8.

In a recent study, García-Berríos et al. synthesized C_nS Au MPCs of various chaing lengths (n = C4–C11) and exposed them to a set of 11 vapor analytes.[49] The authors observed that an increase in the number of carbons in the monolayer showed a proportional increase in sensitivity (drop in current) whereas in the presence of polar vapors sensitivity also increased but responding with an increase in film current. This behavior was previously noted by others and qualitatively attributed to the effects of the dielectric constant of the vapor analyte partitioning into the film. Here, the authors considered that the dielectric ε_s (organic capping + analyte vapor) would be affected by the concentration of vapors in the film (C_f). Based on quartz crystal microbalance (QCM) measurements, the researchers assumed that the vapor analyte partitioned at the organic matrix only and not at the Au core leading to partition coefficient values independent of the monolayer chainlength. They also calculated that an order of magnitude

change in the dielectric value of the film in the presence of the vapor analyte (vapor + organic matrix) showed a small change in response. These data were supported by no change in the plasmon band for a film of C8S Au MPCs exposed to ethanol, suggesting that the dielectric may play a minor role and that interparticle distance or film morphology may be a dominant factor in the sensing mechanism.

Modeling: Zeller and co-workers developed a model relating the chemiresistive response of films of octanethiolate-coated Au MPCs to vapor-film partition coefficients, density of the analyte in the condensed phase, and dielectric constant for 28 different VOCs.[33] Based on these parameters, the model can predict responses within 24%. They found that vapor sensitivities for chemiresistor films of various dimensions were independent of the film volume, although thicker films tend to have lower noise.[34] They observed that the chemiresistor sensitivity was inversely proportional to the partial pressure of the pure analyte. They also observed that the relative resistance change was much higher than the relative mass change for the same VOC concentration. Another interesting result is that the ratio of the sensor response to mass uptake was highest for high density nonpolar vapors and alcohols, with the latter being greatly influenced by the dielectric constant of the vapor.

6.1.2. Drop-Cast Films of Alkylamine-Coated Au Nanoparticles

Briglin et al. studied films of dodecylamine ($C_{12}NH_2$)-coated Au MPCs for the chemiresistive sensing of water, acetone, toluene, and vapors containing alkanethiols of various chainlengths.[37] As expected, the films displayed a reversible decrease in current in the presence of water, acetone, and toluene vapors, consistent with the film swelling mechanism already described. Exposure to the thiol molecules led to irreversible current changes due to the strong covalent S–Au bond formed upon vapor-phase place exchange between the original alkylamines and the incoming thiols. An irreversible current increase occurred in the presence of H_2S (diluted with N_2), CH_3SH, and propanethiol, which is consistent with a decrease in the core-to-core distance after the vapor-phase place exchange between the long C12 alkylamines and the shorter thiol-containing molecules. Interestingly, the film displayed a decrease in current in the presence of the octanethiol vapor for reasons that are unclear since it is still shorter than the original $C12NH_2$ monolayer.

6.1.3. Drop-Cast Films of Organomercaptan-, Organoamine-, or Polymer-Coated Pt Nanoparticles

Haick and co-workers studied the effect of particle shape between cubic and spherical Pt nanoparticles coated with polyacrylate and polyvinylpolyrridone, respectively and compared their sensing attributes towards various VOCs.[90] They conclude that cubic nanoparticles lead to a more sensitive chemiresistive film as compared to spherical nanoparticles. Based on ellipsometry measurements, cubic nanoparticles showed higher swellability which suggests that the dimensions and geometry of the film pores may favor the partition of vapor analytes. Following their report, Dovgolevsky et al. reported on oleylamine (ODA)-coated cubic Pt nanoparticles which were liquid-phase place exchanged with 11-mercaptoundecanol (MUOH), 11-mercaptoundecanoic acid (MUA), and benzylmercaptan (BZM). These MPCs were drop-cast deposited onto IDA electrodes and used as a chemiresistor for the detection of various VOCs including decane, octane, hexane, EtOH, ethyl benzene, and water.[35] They observed that the film of MUA-coated Pt MPCs exhibited a decrease in resistance in the presence of water as previously reported by others.[27,39] They concluded that the nonpolar organic shell was more responsive to nonpolar analytes and less responsive to polar vapors such as ethanol and water. Importantly, the ODA-coated film of Pt MPCs detected nonpolar vapors (i.e., octane and decane) at high humidity (81% RH) under ambient conditions.

6.1.4. Drop-Cast Films of Surfactant-Coated Au and Alloy Nanoparticles

Our group recently synthesized and prepared films of tetraoctylammonium bromide (TOABr)-stabilized Au and AuAg alloy nanoparticles and compared their chemiresistive response to more conventional films of hexanethiol (C6S)-coated Au MPCs.[38] **Figure 6** shows the current–time plots of films of TOABr Au nanoparticles and C6S Au MPCs upon exposure to alternating flows of N_2 and MeOH, EtOH, IPA,

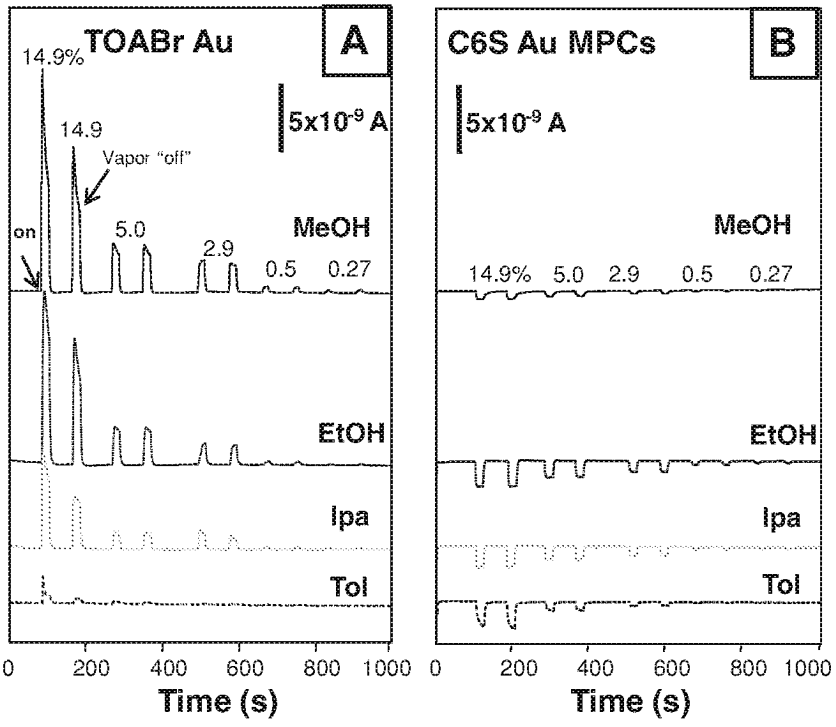

Figure 6. Current–time plots for films of A) TOABr Au nanoparticles and B) C6S Au MPCs film exposed to MeOH, EtOH, IPA, and toluene (Tol) from 14.9 to 0.27% vapor concentration as indicated. Response profiles are offset for comparison. Reproduced with permission.[38]

acetone, and toluene from 14.9 to 0.27% vapor concentration. Upon exposure to polar and nonpolar vapors, the films exhibited an increase in current, in contrast to the usual decrease in current, and a better sensitivity to polar analytes (≈30–150 times lower limit of detection). The lowest limit of detection (LOD) achieved with the film of TOABr-coated Au nanoparticles was 2 ppm for EtOH. The sensing mechanism is not fully understood but may involve Faradic or capacitive charging current as opposed to electron hopping only. We observed that the films of TOABr-coated AuAg (Ag < 10%) alloy nanoparticles drastically reduced the vapor sensitivity, demonstrating that the metal composition may play an important role other than just serving as a conductive pathway.

6.2. Chemically Linked 3D Films of Au Nanoparticles

6.2.1. Dithiol and Hydrogen-Bonding Linkages

Effect of Particle Size: Usually the synthesis of MPCs following the Brust–Schiffrin procedure leads to somewhat polydisperse nanoparticles. There are two reports[39,91] that explored the sensing behavior for films comprised of different, more uniform particle sizes prepared by post synthesis thermal treatment.[92] Zhong and co-workers synthesized C12S Au MPCs of 1.9 ± 0.7 and 5.2 ± 0.3 nm through a modified Brust method followed by thermal treatment.[66] The two different batches of MPCs exhibited monodispersity above 80% of the population. The thermal treatment led to an annealing of the nanoparticles, resulting in an increase in their size and change in shape with no evidence of thermal desorption of the monolayer.[70] They deposited the MPCs as films across electrodes by cross-linking the MPCs with 1,9-nonanedithiol and 11-mercaptoundecanoic acid directly in solution through a place exchange cross-linking precipitation mechanism.[93] **Table 2** shows the shell linkage, vapors tested, and response sensitivity data for the two different core size nanoparticle films. The table indicates that there are similarities and differences between the two types of films. The sensitivity of the films of 5 and 2 nm MPCs with the same linker, as indicated by the slopes of the calibration curves, were similar in the presence of hexane while the 5 nm nanoparticles responded better to toluene. The response to polar analytes was smaller for films of both MPCs due to the nonpolar nature of the protecting ligands. The researchers observed an increase in current in the presence of polar vapors for the 2 nm particle film similar to the behavior observed previously by Wohltjen[27] and Evans.[86] They attributed the increase in current to the higher dielectric constant of the vapor analyte, which dominated the response over film swelling. For instance, the 2 nm film displayed a current increase in the presence of MeOH and the usual current decrease in the presence of more hydrophobic vapors (propanol and butanol). The authors suggest that this unusual behavior depends on changes in hydrophobicity in the film, the type of organic linker, vapor loading, film thickness, and to a lesser extent on the MPC size. The correlation between core size and sensing was still unclear.

Table 2. Response sensitivity for different vapor sorption at films comprised of 2 and 5 nm particles with different shell linkers. Note: water = Wa, hexane = Hx, toluene = Tol. Reproduced with permission.[39]

Shell linkage	Vapor	Responses for different core sizes			
		$Au_{5\ nm}$		$Au_{2\ nm}$	
		$(\Delta R/R_i)/\Delta C$	$\Delta f/\Delta C$	$(\Delta R/R_i)/\Delta C$	Df/DC
MUA	Tol	2.24×10^{-3}	−0.24	8.28×10^{-4}	−0.23
	Hx	4.17×10^{-4}	−0.042	1.87×10^{-4}	−0.030
	MeOH	7.04×10^{-5}	−0.010	b)	–
	Wa	2.96×10^{-5}	−0.014	b)	–
NDT	Tol	2.71×10^{-4}	−0.18	3.14×10^{-4}	−0.24
	Hx	$5.23 \times 10^{-5a)}$	−0.028	$5.49 \times 10^{-5a)}$	−0.036
	MeOH	1.89×10^{-5}	–	b)	–
	Wa	1.11×10^{-5}	–	b)	–

a)Slopes from linear approximations; b)No entry due to unusual response profiles.

Recently, Wang et al. reported a chemiresistor sensor array comprised of a film of linked and unlinked Au MPCs.[40] Dithiol and MUA crosslinking were performed by an exchanging-crosslinking-precipitation route and the film assembled via stamping procedures on a flexible polyethylene terepthalate (PET) substrate.[91] They studied the electrical conductivity of monodisperse mercaptoundecanoic acid (MUA)-, 1,9 nonanedithiol (NDT)-, and decanethiol (DT)-coated Au nanoparticles of 2 and 7 nm diameter towards the presence of benzene, hexane, toluene, and water. The flexible platform proved to be tolerant to multiple bending cycles with little or no signal interference. The final response of these films to VOCs correlates well with the combination of particle size, dielectric medium, and substrate-film interaction. A comparison between MUA-coated Au MPC films of 2 and 7 nm showed that the film of smaller nanoparticles was slightly less responsive to all organic vapors except for toluene; while polar vapors with large dielectric constant (i.e., water) displayed a negative response (resistance decrease). The authors speculated that larger nanoparticles (lower percentage of organics) with higher initial conductivity may lead to larger sensitivity to vapors of low dielectric constants. On the other hand, an increase in dielectric constant at 2 nm diameter nanoparticle films reversed the response direction.

Effect of Linker Chainlength: Vossmeyer and co-workers prepared films of assembled Au nanoparticles by sequential dipping of the electrodes into solutions of $C12NH_2$ Au MPCs and alkanedithiols of various chainlength (C6, C8, C12, and C16). They demonstrated that the dithiols completely replaced the $C12NH_2$ ligands and that the chemiresistor response increased exponentially with increasing organic chainlength.[67] Later, Zhong and co-workers prepared films of C12S Au and AuAg MPCs that were assembled by a one-step exchange-crosslinking-precipitation route with dithiols of different chainlengths (C6, C9, C12, and C16) and monitored their conductivity and vapor response upon exposure to toluene, hexane, and benzene vapors.[40] Their study confirmed the work of Vossmeyer, showing that the conductivity of films of nanoparticles decreased as the chainlength of the linker ligands increased and that the device sensitivity increased with increasing interparticle distance (length of the

linker molecule), showing that the films can be fine-tuned at the molecular level.

Effect of Film Flexibility: The most common sensing mechanism for the detection of VOCs with films of metal MPCs is the vapor-induced swelling mechanism, which leads to a resistance increase in the film. Film flexibility is consequently an important variable, since the ability of a film to swell is closely related to its flexibility. While this is intuitively important, several reports appeared in this field before it was addressed experimentally. Murray and co-workers recognized the importance of flexibility in the sensing behavior of metal ion–carboxylate linked Au MPC films for VOC sensing.[44] The results of Vossmeyer and Zhong describing the effect of linker chainlength in VOC sensing as discussed in the previous section is likely due in part to flexibility, but this variable was not directly addressed in these early studies.

Our group directly studied the effect of film flexibility on VOC sensing with films of Au MPCs by altering the degree of dithiol cross-linking in microscale films of C6S Au MPCs and measuring their chemiresistive response towards saturated toluene and 2-propanol vapors.[41] The devices were prepared by microcontact printing the small MPC films between a pair of electrodes. Cross-linking of these microscale films was necessary for film stability. We cross-linked the films by exposing them to hexanedithiol vapor for various amounts of time, which led to Au MPC–[S–$(CH_2)_6$–S]–Au MPC linkages in the film, prior to VOC sensing. The current-time plots in **Figure 7**A show the response to saturated toluene for films that were cross-linked by exposure to hexanedithiol vapor for 1, 30, and 60 min. The data clearly show that the response to toluene dramatically decreases from 61% down to 8% as the exposure time to dithiol vapors increases. We attribute the decrease in response to a reduction in film flexibility that occurs with a larger degree of cross-linking with longer exposure time to hexanedithiol. This report clearly demonstrated the importance of film flexibility in chemiresistive sensing with organic-modified metal nanoparticles in a controlled manner.

In a later study, Vossmeyer and co-workers elegantly studied the effect of film flexibility for films of Au MPCs assembled in a layer-by-layer fashion, where the film was alternately exposed to a dithiol linker and $C12NH_2$-coated Au MPCs to build up the layers in the film.[94] The thiol groups in the bifunctional linker easily displace the $C12NH_2$ to allow the assembly. They compared the conductivity and chemiresistive sensing properties of films prepared using 1,12-dodecanedithiol (DDT), [4]-staffane-3.3‴-dithiol (SF4), and 4,4′ terphenyldithiol (TPT). The DDT is a long, flexible linker while both SF4 and TPT are rigid linkers, with the latter having a high conductivity due to delocalization of electrons in the molecule. Figure 7B,C shows the chemiresistive and quartz crystal microbalance (QCM) response of the three films exposed to 5000 ppm toluene, 4-methyl-2-pentanone, 1-propanol, and water, which have dielectric constants of 2.4, 13.1, 20.8, and 80.1, respectively, but similar vapor pressures. The more flexible DDT-linked films responded with the largest increase in resistance, which is the response direction expected for the vapor-induced swelling mechanism.

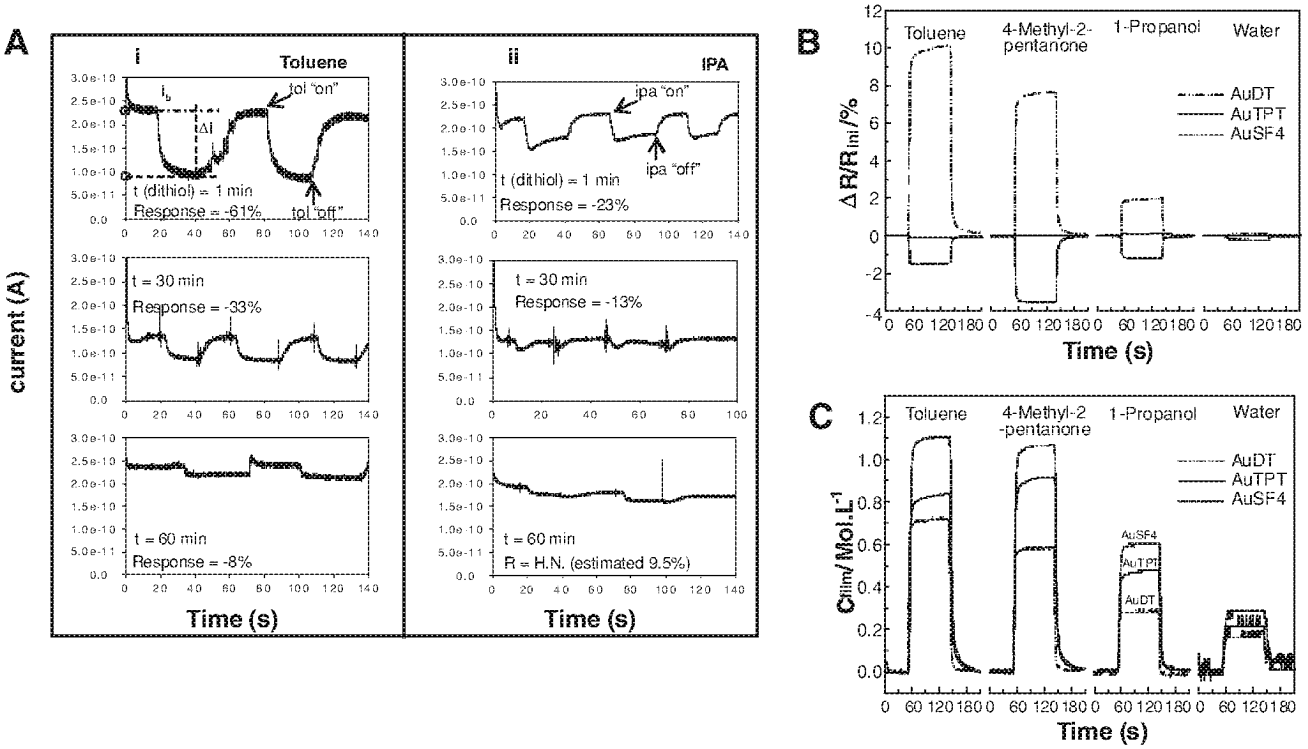

Figure 7. A) Current–time plots showing the response of C6S Au MPC microfilms to saturated i) toluene and ii) IPA as a function of exposure time to hexanedithiol during cross-linking. B,C) Response profiles of AuDT (._._.), SF4 (….), and AuTPT (_) toward 5000 ppm of the indicated analytes. Reproduced with permission.[A][41][B,C][94]

Interestingly, the SF4-linked film exhibited a decrease in resistance and there was no change in resistance for the TPT-linked film, despite the significant uptake of analyte observed by QCM. The response of the DDT-linked films increased with decreasing dielectric constant of the vapor analyte, consistent with greater mass uptake and film swelling when there is a match in polarity between the film and the analyte. In the case of the rigid SF4-linked film, the response is dominated by a change in the dielectric constant of the medium surrounding the nanoparticles in the presence of the vapor molecules since there is little or no vapor-induced swelling. Accordingly, the resistance decreased with increasing dielectric constant of the analyte. The response to 4-methyl-2-pentanone (≈4%) was approximately three times larger than the response to toluene at similar mass loadings in the film. In the case of the rigid, highly conductive TPT-linked film, there is no film swelling and the large conductance negates any potential effect from altering the dielectric constant of the environment. This important study clearly separated out the swelling from the dielectric change mechanisms, confirmed film loading by QCM, and showed the importance of linker rigidity. In addition, this paper demonstrated that the electronic properties of highly conductive molecules are not very sensitive to vapor phase analyte interactions, which is somewhat analogous to the fact that highly conductive metal nanowires are usually not as sensitive to their environment as semiconductor nanowires.

Guo et al. prepared films of C8S Au MPCs and crosslinked them with hexanedithiols and benzenedimethanethiol via one-step exchange-cross-linking self assembling route.[50] Part of the as-synthesized Au MPCs were purified in a liquid–solid chromatography column and the rest of the nanoparticles were kept before crosslinking with dithiols. Purified and as-prepared films were exposed to water, Tol, ethyl acetate, IPA, EtOH, and acetonitrile for chemiresistive sensing. The authors observed that as-prepared films were more responsive to toluene than linked films following the order of C8S > hexanedithiol > benzenedimethanethiol. In this report the authors also observed that as-prepared films were less responsive to all vapors tested and that the fim resistance changed from an increase to a decrease as the relative humidity concentration increased.[95] They attributed this behavior to the presence of ionic impurities coming from the tetraoctylammonium bromide (TOABr) residue usually present in the Brust–Schiffrin two-phase synthesis.

More recently, Toda et al. studied vapor-induced swelling as determined by monitoring the mechanical deflections of a cantilever coated with an Au MPC film.[42] The films were assembled via layer-by-layer deposition of $C12NH_2$-coated Au MPCs using terphenyldithiol (TPT) as a cross-linker onto 1) a bare Au-coated cantilever and 2) a 3-aminopropyldimethylethoxysilane (APDMES)-coated cantilever and exposed both films to toluene vapors. They found that the transduction of swelling into a mechanical deflection was more pronounced on Au MPC films deposited on the APDMES-functionalized cantilever as compared to those deposited on the Au-coated cantilever. The authors suggest that the weaker interaction at the Au MPC/APDMES interface allows more mobility compared to the stronger, covalently-linked Au MPC/TPT/Au film interface. While this study does not involve chemiresistive sensing, it shines light on the importance of the film/substrate interface in vapor-induced film swelling.

Effect of Film Thickness and Structure: Vossmeyer and coworkers studied the influence of both film thickness and structure on the vapor response of dithiol-linked Au nanoparticle films.[96] The cartoon in **Figure 8** illustrates the layer-by-layer deposition of Au nanoparticles with 1,12-dodecanedithiol (DDT) as described previously and the corresponding *I–V* characteristics before assembly (a), at an intermediate stage in the assembly (b), and after the film surpasses the

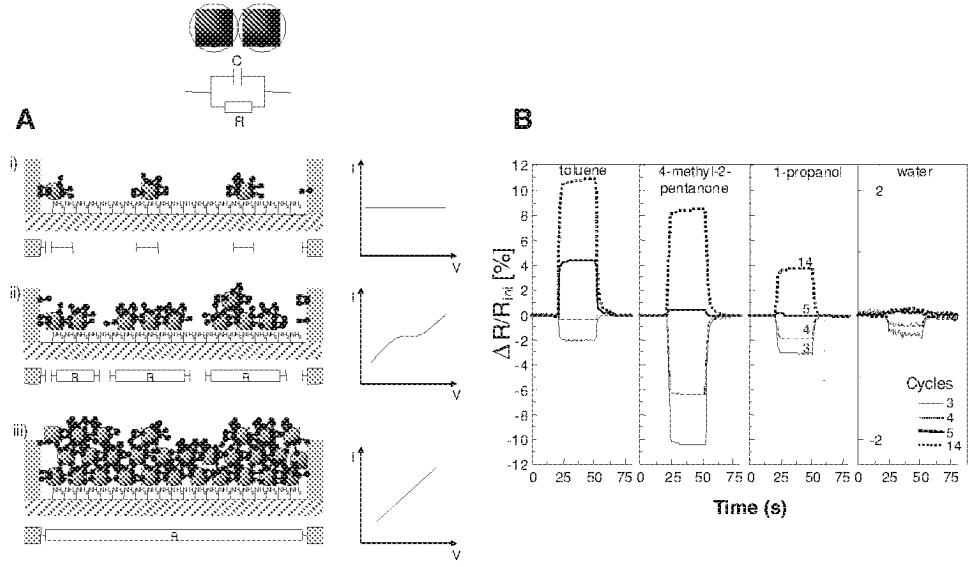

Figure 8. Model for film growth: a) island nucleation and growth, b) before and c) after the percolation threshold. *I–V* curves showing the different stages from nonconductive to conductive films are to the right, response profiles of the films exposed to 5000 ppm of toluene, 1-propanol, 4-methyl-2-pentanone, and water with the indicated number of cycles are shown below. The response profiles move from negative to positive ($\Delta R/R_{ini}$) values as the number of cycles increases. Reproduced with permission.[96]

percolation threshold (c). The top illustration in Figure 8 depicts two spherical nanoparticles coated with an organic material, resembling a circuit of a capacitor in parallel with a resistor. As discussed in Section 4, the stabilizer acts as the dielectric medium and the nanoparticles as the plates in the capacitor. As the film grows thicker, the distance between islands becomes small enough to allow electron transport. If the nanoparticle capacitance is sufficiently low that the electron transport barrier height is larger than kT, then coulomb blockade or staircase behavior may be observed as represented by steps or a single plateau in the I–V curve. As the film grows even thicker, the inter-island distance decreases further and the number of pathways increases, leading to more ohmic behavior as represented by a linear I–V curve. The bottom part of Figure 8 shows the response of films with different thicknesses, as controlled by the number of nanoparticle deposition cycles, following exposure to toluene, 4-methyl-2-pentanone, 1-propanol, and water. The response trend changes from a negative response (resistance decrease) to a positive response (resistance increase) as the number of deposition cycles increases and the film becomes thicker. At low coverage (island-like film) the authors suggest that the decrease in resistance is due to swelling of the film which somehow leads to a reduction in the distance between islands. A decrease in resistance occurred even when the film was exposed to toluene, whose permittivity value (2.38) is similar to the linker (2.01), ruling out the possibility of changes in the dielectric causing the resistance decrease. Island-like films before reaching the percolation threshold (Figure 8b) swell in all directions (except towards the substrate) leading to a reduced space between islands and therefore improved conductivity in the presence of vapors. On the other hand, thicker 3D films swell normal to the plane of the substrate leading to an increased resistance due to the increased separation between nanoparticles. This in part explains the resistance increase in the presence of polar and nonpolar vapors for thicker films. The authors conclude that structure and thickness of the film play a crucial role in the sensing mechanism.

Zhong and co-workers examined the effect of film thickness on vapor sorption for films of C12S Au MPCs linked with 1,9-nonanedithiol by cross-linking precipitation.[39] They used a QCM and resistance measurements to test the film response towards hexane vapor. They prepared 7–22.2 equivalent layer films and observed small changes in resistance sensitivity and frequency sensitivity. The resistance sensitivity increased by a factor of 1.3 from 7 to ≈16 layers while frequency changes (mass) exhibited an increase by a factor of 2.5 up to 9 equivalent layers. The authors concluded that at about 8 equivalent layers, the vapor might not further penetrate the film, indicating that the resistance change sensitivity is insignificant once the film reaches a certain thickness. The different result compared to Vossmeyer and co-workers is likely due to the fact that the films were all above the percolation threshold in this study.

6.2.2. Metal Ion–Carboxylate Linkages

Murray and co-workers studied chemiresistive films of Au MPCs protected with a mixed monolayer of alkanethiolates and carboxylic acid functionalized alkanethiolates that were linked together in the film by a network of carboxylate–M^{n+}–carboxylate bridges, where M^{n+} was Cu^{2+}, Zn^{2+}, Ag^{+}, or methyl viologen.[44,45] These network polymer films exhibited a decrease in current in the presence of ethanol and dichloromethane vapors.[45] The current response to dichloromethane was the smallest for films linked with Ag^{+} compared to those linked with Zn^{2+} and Cu^{2+} ions. They attributed the smaller response of films linked with Ag^{+} to short core-to-core distances as confirmed by larger initial conductivity and profilometry measurements.[45] The conductivity and chemiresistive response for films comprised of Au MPCs linked by carboxylate–Cu^{2+}–carboxylate bridges with different chainlengths in the alkanethiolate ligands and in the COOH-functionalized ligands showed different chainlength-dependent conductivity and vapor sensing characteristics as discussed in the next section.[44]

Effect of Film Chain Length: Zamborini et al. prepared films of Au MPCs protected with mixed monolayers of alkanethiolate ($[S–(CH_2)_n–CH_3]$, denoted C(n+1)) and ω-carboxylic acid alkanethiolate $[S–(CH_2)_m–COOH]$ ligands through a layer-by-layer procedure resulting in MPCs linked by carboxylate–Cu^{2+}–carboxylate bridges.[44] They synthesized pure alkanethiolate-coated Au MPCs of varying chainlength (C4, C6, C8, C10, and C12) first and performed a place exchange reaction between the n-alkanethiolates initially surrounding the clusters and ω-carboxylic acid alkanethiolates to form the mixed monolayer MPCs, which were on average 1.6 nm in diameter and contained 15–20 ω-carboxylic acid alkanethiolate ligands out of a total of about 53 ligands. The COOH-terminated thiols studied were mercaptohexanoic acid (MHA), mercaptoundecanoic acid (MUA), and mercaptohexadecanoic acid (MHDA). The magnitude of the conductivity change of these films in the presence of EtOH and dichloromethane depended on the number of methylene groups in the alkanethiolate (n = 3,5,7,9,11) and in the ω-carboxylic acid alkanethiolate (m = 5,10,15) ligands.[44] **Figure 9** shows the device current and the QCM as a function of time for a film of C6/MUA Au MPCs in the presence of alternating flow of pure N_2 and different concentrations of EtOH in N_2 carrier gas. The current decrease in the presence of EtOH due to film swelling correlates with the mass increase in the film as EtOH partitions into the film. The magnitude of the current and mass response was proportional to the EtOH concentration (or partial pressure). **Table 3** shows the response in terms of percent current change (%ΔI), QCM frequency change (-Δf, Hz), amount of EtOH absorbed (nmol), response time based on 90% of the current response, and QCM response time (s) for several different films of MPCs coated with the different combinations of alkanethiolates (nonlinker ligand) and ω-carboxylic acid alkanethiolates (linker ligand) upon exposure to saturated EtOH vapor. One can conclude from the table that the %ΔI correlates well with the mass loading values measured for C4/MUA, C6/MUA, and C10/MUA. Also, the magnitude of the response was largest for the films of MPCs with the largest difference in chainlength between the non-linker and linker ligands. For example the film of C4/MHDA Au MPCs (difference of 12 carbons) exhibited an 83% current decrease, whereas the film of C4/MHA Au MPCs (different of 2

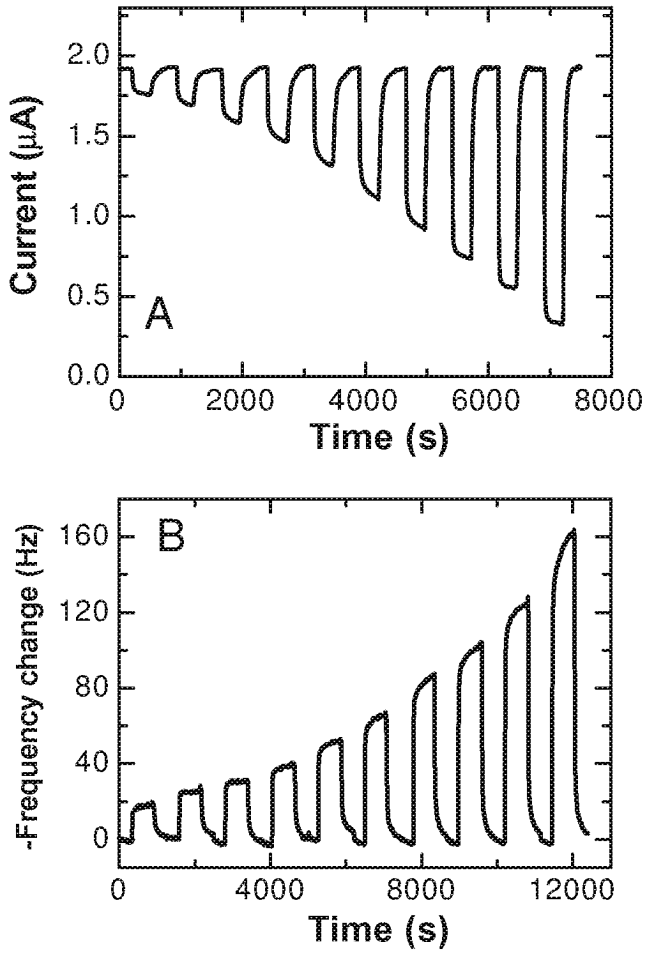

Figure 9. A) Current–time and B) QCM plots showing changes in current and frequency, respectively of a C6 MUA film exposed to different ethanol vapor concentrations. Reproduced with permission.[44]

carbons) exhibited a 51% current decrease in the presence of equal concentrations of EtOH. The larger response for the biggest chainlength mismatch was likely due to a more open structure for ethanol partitioning and greater film flexibility.

Table 3. Response of network nanoparticle films to saturated (7.9 kPa) ethanol vapor. Note: 11-mercaptoundecanoic acid = MUA, 6-mercaptohexadecanoic acid = MHA, 16-mercaptohexadecanoic acid = MHDA. Reproduced with permission.[44]

MPC Film	%ΔI	$-\Delta f$ [Hz]	Ethanol Absorbed [nmol][a)]	ΔI Response Time [s]	QCM Response Time [s]
C4/MUA	72	150	65	47	192
C6/MUA	75	156	68	8	-
C10/MUA	33[b)]	100	43	13[b)]	168
C4/MHA	51[b)]	na	na	9[b)]	na
C4/MHDA	83[b)]	na	na	7[b)]	na

[a)]Calculated from the Saurbrey equation, assuming absence of viscoelastic effects. The change in volume upon partitioning of ethanol vapor is estimated to be ≤5%. Viscoelastic effects, expected to be negligible with these films at low vapor pressures, will be explored further in a subsequent report dedicated to vapor response; [b)]Obtained in a different flow cell.

6.2.3. Dendrimer-Linked Au Nanoparticles

Vossmeyer and co-workers studied the chemiresistive response of films of Au nanoparticles linked together with various dendrimers of different chemical composition and generation.[43,46,97,111,112] They prepared the films by first synthesizing dodecylamine-stabilized Au MPCs and then assembling the films in a layer-by-layer fashion by repeated deposition cycles involving dipping the electrode substrate into alternating solutions of the MPCs and disulfide polyphenylene (PPh), polyamidoamine (PAMAM), and poly(propyleneimine) (PPI) dendrimers. Exposure of a dendrimer-coated surface to the Au MPCs results in attachment of the Au MPCs to the peripheral groups of the dendrimers by exchange of the $C12NH_2$ ligands with the dendrimer. Subsequent exposure to a dendrimer solution leads to deposition of dendrimer onto the MPCs again by the dendrimer replacing the $C12NH_2$ ligands on the Au MPCs. Continuing this process leads to multilayer (Au nanoparticle/dendrimer)$_n$ films. The films have good mechanical stability with a large number of active sites for analyte interaction due to the presence of the dendrimers.[46] **Figure 10** shows the response profile of films of Au/PPh, Au/PPI, and Au/PAMAM exposed to toluene, 1-propanol, and water vapors. The selectivity correlates well with the polarity of the films and analyte, where the nonpolar PPh and PPI dendrimer films respond best to the nonpolar 1-propanol and toluene vapors, while the film with the polar PAMAM dendrimers responded best to water.[46]

6.2.4. Chemically Linked Films of Other Metal Nanoparticles

Au is by far the most common chemically modified metal nanoparticle used in chemiresistive sensing applications. There are a few reports involving films of metal nanoparticles different than Au, however, it is not well-known if the metal composition plays a role in the sensing attributes or if it just acts as a conductive medium for electron transport. Vossmeyer and co-workers[47] synthesized $C12NH_2$ Pt and Au nanoparticles linked with 1,9-nonanedithiol and exposed them both to the same concentration of water and toluene vapor. They explored the possible binding sites of the vapor analytes on the MPCs. They observed qualitatively that the films responded by an increase in resistance for all vapors but surprisingly, the Pt-containing film responded 2–8 times more than Au, implying that the metal composition does plays an important role, although the details are not well understood.

Zhong and co-workers fabricated sensor arrays consisting of films of C12S Au and C12S AuAg alloy MPCs with controlled spatial properties and thickness.[40] The researchers controlled the spacing between the MPCs and the film thickness by controlling the length of the alkyl mediators (X–$(CH_2)_n$–X) and the number of deposition cycles, respectively as discussed above. They believe that the interparticle chain–chain cohesive interdigitation and chain–vapor interaction determines the relative change of electrical conductivity of the film. However, it was difficult to draw conclusions about the role of metal composition on the chemiresistive attributes.

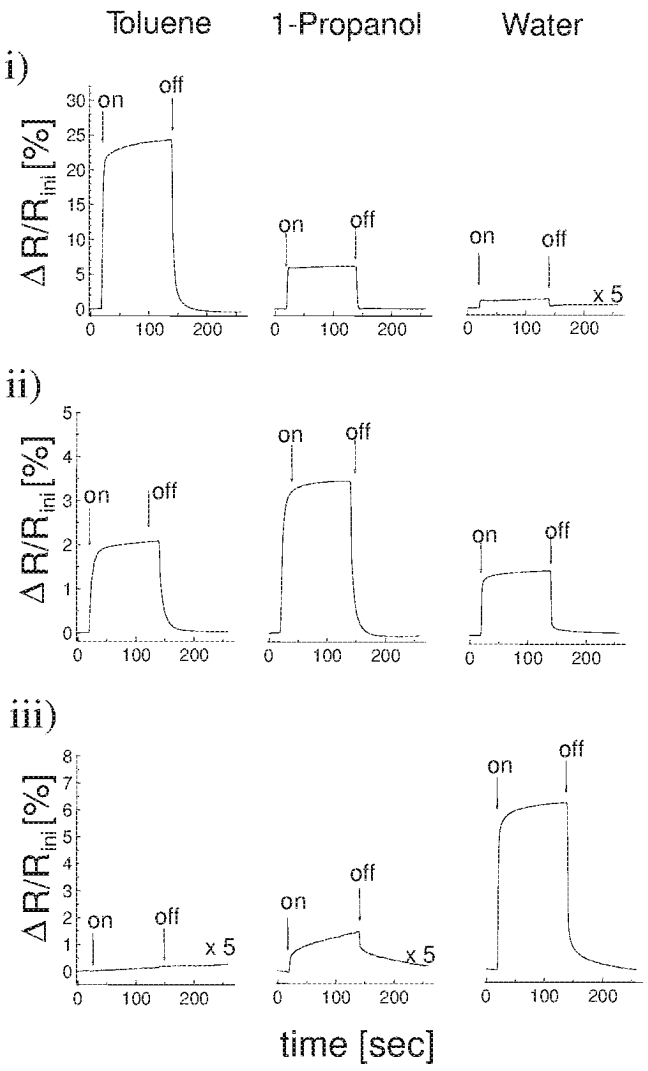

Figure 10. Average percent response to toluene, 1-propanol, and water for dendrimer-coated Au nanoparticle films of i) Au/PPh, ii) Au/PPI, and iii) Au/PAMAM. Reproduced with permission.[46]

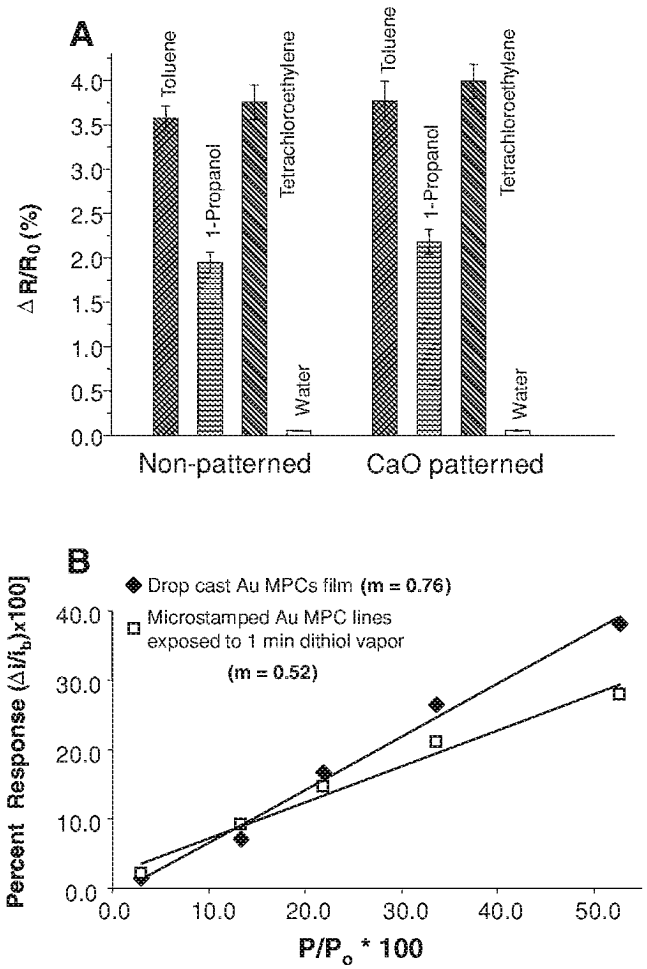

Figure 11. A) Average percent response plot for patterned and nonpatterned films upon 2500 ppm at the indicated vapors. B) Slopes of a large drop-coated and microlines of C6S Au MPCs taken form the exposure of the films to IPA at the indicated concentrations (Zamborini's group, unpublished results). Reproduced with permission.[78]

6.3. Patterned 3D Films of Metal Nanoparticles

Miniaturization of MPC films down to the micro- and nanoscale is important for practical reasons, such as increased portability for field testing, detection in highly confined regions, reduced cost, and the fact that multiple sensors could be fabricated on one device for pattern recognition analysis or multianalyte detection. Fundamentally, it is also interesting to study the sensing properties of smaller films compared to larger films to determine if the properties change with size reduction. There are five reports that explore the miniaturization of MPC films for chemiresistive vapor sensing.[33,34,41,78,79]

Harnack et al. explored the chemiresistive sensing of small films of $C12NH_2$ Au MPC films cross-linked with 1,9 nonanedithiol and compared it to larger films of the same MPCs.[78] To reduce the size of the film, they used conventional photolithography techniques based on a water-soluble mask. Briefly, they deposited a thin Ca layer on top of the Si substrate followed by oxidation of Ca to CaO and $Ca(OH)_2$, which constitutes the water soluble mask. They then spun a photoresist on top of the mask and patterned it using photolithography or electron-beam lithography. The unprotected mask areas were etched away by adding H_2SO_4 and the resist layer was removed with acetone without affecting the water soluble mask. Finally, the substrate was coated with silane groups, which preferentially bind to the Si/SiO_x part of the wafer. Deposition of the nanoparticles then was performed and the mask dissolved away leaving behind patterns as small as ≈30 μm. **Figure 11**A shows the percent response for patterned microscale films and non-patterned larger films averaged from twelve and six films, respectively, upon exposure to 2500 ppm of the various vapors as indicated. From the figure, one can conclude that there is no apparent difference in percent resistance between patterned and nonpatterned films.

Ibañez et al. fabricated microscale films of C6S Au MPCs by microcontact printing.[41] Briefly, a patterned

polydimethylsiloxane (PDMS) stamp with featured lines was inked with a solution of C6S Au MPCs, allowed to dry for a few minutes, and brought into conformal contact with a solid substrate containing two electrodes separated by 1 μm. Removal of the MPC inked PDMS stamp left behind a patterned film of MPCs with feature sizes corresponding to the stamp features. We observed that microscale films of MPCs were unstable in the presence of saturated vapors of solvents that they are soluble in, such as toluene. This led to distortion of the patterned microfilms and the loss of a conductive pathway. To improve stability, we crosslinked the films by exposure to hexanedithiol vapor for 1, 15, or 30 min. Figure 11B shows the slopes of a microstamped film stabilized by 1 min hexanedithiol exposure and a large drop-coated C6S Au MPC film measured from the percent response of the film in the presence of IPA vapor of different concentrations as noted. The sensitivity of the microfilm is lower compared to the large film because it had to be cross-linked with the hexanedithiol for 1 min for stability (vide supra). This increased the film rigidity and slightly lowered the sensitivity, but it is necessary since nonlinked microscale films became irreversibly distorted and lost conductivity. Overall, the sensing behavior of microscale films with minimal cross-linking is comparable to that of larger films as shown in Figure 11.

Raguse et al. inkjet-printed films of C6S MPCs for detecting organic analytes dissolved in ionically conductive electrolyte solution.[79] The small size films were assembled in order to reduce the double layer capacitance and measure impedance through the film as discussed later in Section 7.

Zellers and co-workers studied the chemiresistive vapor response of miniaturized films ranging from 0.001 to 1.7 mm^2.[33] The smaller devices displayed faster response times without loss of sensitivity and the authors projected that the low limits of detection (ppb range) observed for low vapor pressure analytes on larger sensors should be similar on miniaturized sensors. The same group later reported the fabrication of the smallest chemiresistive vapor sensor based on films of Au MPCs prepared by electron beam induced cross-linking.[34] These devices responded fast and reversibly to very small samples of analyte with similar sensitivities as larger devices, showing their promise in microanalysis systems, such as μGC. However, the authors did not discuss the effect that crosslinking may have on film flexibility and vapor response.

6.4. 2D Nanoparticle Films

Hanwell et al. prepared Langmuir–Schaeffer films comprised of two or more monolayers thick of thiol-coated Au MPCs for studying the conductivity of the film as a function of temperature and determining the vapor and gas sensing properties.[52] They examined 2D Au nanoparticle films functionalized with 1-hexanethiol, 1-dodecanethiol, and 4-methylbenzenethiol and exposed them to small concentrations of toluene (1.0 ppt). They observed that C10S Au MPC films displayed no dc current, presumably due to the long chainlength and the low film coverage inhibiting electron tansport through the film.[96] For that reason, the authors used C6S Au MPC films 8 layers thick to be able to obtain direct current and perform the experiments. The response to toluene was more pronounced for Au nanoparticles coated with aromatic thiols than alkanethiols, indicating the importance of the monolayer functionalization on the sensor response. Finally, the conductivity of the film always decreased in the presence of toluene indicating that swelling of the film was the dominant mechanism.

6.5. Individual Nanoparticles

There is one example in the literature describing the single electron tunneling (SET) of solid-state individual nanoparticles for vapor sensing. Chen and co-workers[53] recently conducted scanning tunneling spectroscopy (STS) experiments in combination with scanning tunneling microscopy (STM) on single organic-coated nanoparticles of various sizes and exposed them to hexane, toluene, ethyl ether, chloroform, dichloromethane, and acetone. They immobilized C6S Au MPCs onto a SAM-modified Au surface and imaged it with a Pt/Ir tip scanning on top of the MPCs. They analyzed changes in the particle charging energy and the charge transport across the tip/particle/substrate for different particles sizes in the presence of VOCs. **Figure 12** shows the Coulomb blockade and Coulomb staircase phenomenon for nanoparticles of 3.2, 6.3, and 11.8 nm diameter in the presence of N_2 and alternating concentrations of hexane as indicated. They also performed the control experiment without nanoparticles for comparison. As described in Section 4, when a bias is applied across a nanoparticle junction, if the capacitance of the nanoparticle is small and the charging energy ($e^2/2C$) is larger than kT, then the I–V curve exhibits Coulomb blockade behavior. It is clear from the figure that the Coulomb gap is a function of the nanoparticle size and the dielectric medium, where changes in the latter are due to vapors partitioning into the junction. For instance, a junction formed with a small nanoparticle (≈3 nm dia.) exhibited a relatively large Coulomb blockade which slighlty increased in the presence of organic vapors. In contrast, large nanoparticles (11.8 nm diameter) exhibited higher conductivity and staircase behavior that was not modified significantly by vapors. Intermediate-sized MPCs (6.3 nm diameter) were the most responsive to the presence of vapors leading to a wider Coulomb blockade gap (voltage width) as the vapor concentration increased and as the vapor polarity decreased. Since the intermediate-size nanoparticle was the most responsive, researchers exposed the 6.3 nm particle to different vapors in order to study the changes in the dielectric medium. A close examination of the intermediate nanoparticles indicated that that they were more responsive to nonpolar vapors compared to polar ones. The authors suggest that there are swelling effects when the vapor penetrates the organic monolayer and SAM, leading to changes in resistance and organic chain structure. These two variables may impact the impedance measurements leading to a wider Coulomb gap in the presence of nonpolar organic vapors as compared to polar vapors.

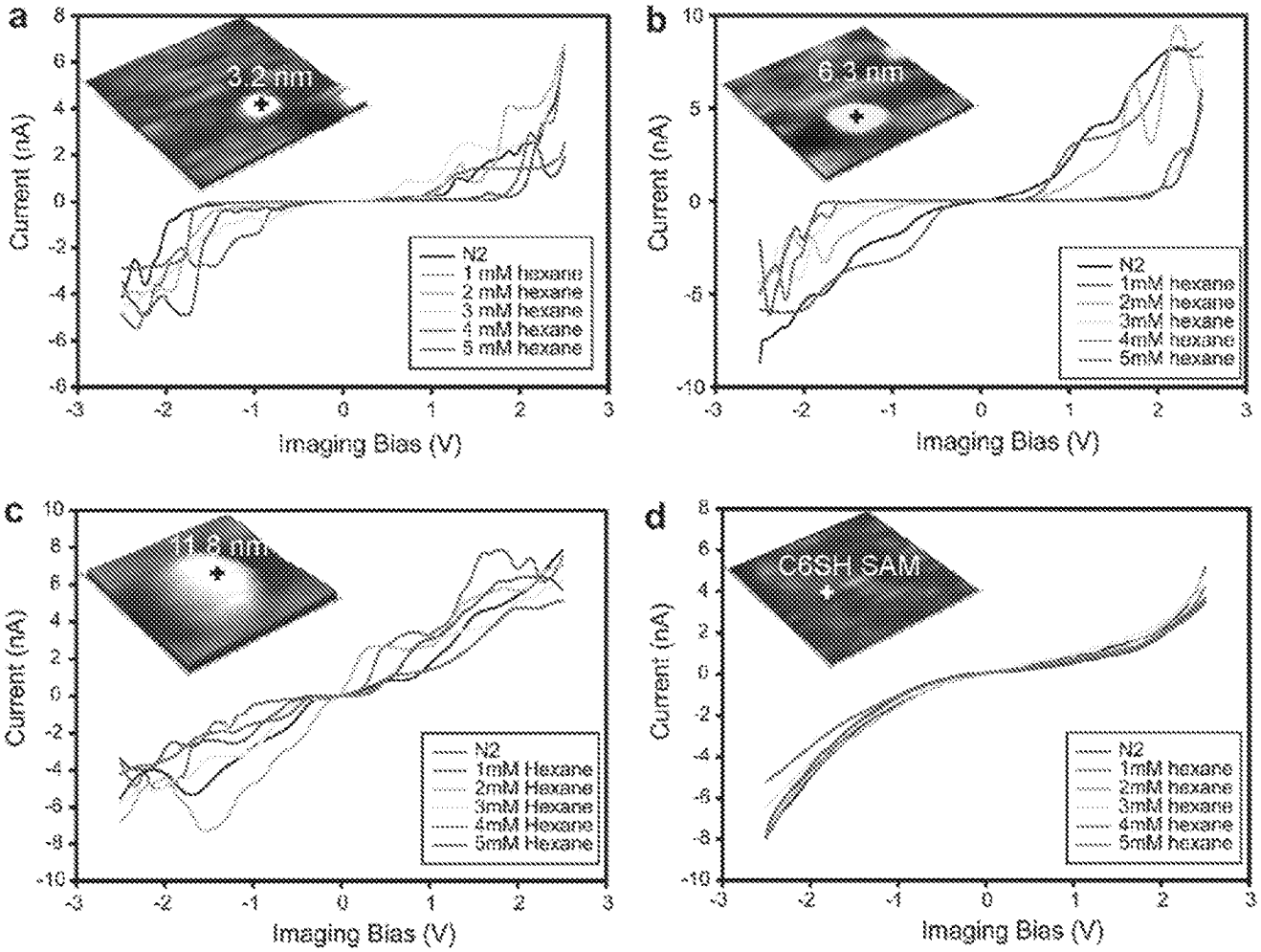

Figure 12. a,b,c) STS of single hexanethiol-coated Au nanoparticles of different sizes exposed to various concentrations of hexane solvent as noted and d) control experiment. Reproduced with permission.[53]

7. Chemiresistive Sensing of Gases

7.1. Drop-Coated 3D Films of Metal Nanoparticles

7.1.1. Organomercaptan-Coated Nanoparticles

Our group studied the chemiresistive sensing of H_2 gas with films of C6S Pd MPCs.[75] It has been well-established that Pd metal can react directly with H_2 to form PdH_x. The H–H bond first dissociates and adsorbs onto the Pd surface and then the H atoms can diffuse into the bulk Pd lattice. This leads to a volume expansion, larger lattice constant, and decrease in conductivity for bulk films. For films of separated Pd nanoparticles or disconnected Pd nanowires,[83] the volume expansion can lead to a more connected film with an increase in the conductivity. We initially studied the conductivity response of films of C6S Pd MPCs to H_2 gas. Films of C6S Pd MPCs were fairly nonresponsive in the presence of H_2, likely due to the thiols blocking the Pd surface, preventing interaction with the H_2 gas. These films exhibited very small, irreproducible and irreversible conductance increases and were deemed unsuitable for sensing applications. Subjecting the films to ozone or high temperature treatment promoted the Pd-H reaction through partial desorption of the C6S monolayer. These treatments eventually led to a sensitive and stable H_2 sensor, but with a different response. Ozone treatment followed by exposure to 100% H_2 led to a fast and reversible increase in current for concentrations as low as 1100 ppm H_2. Temperature treatment led to a current increase or decrease, depending on the temperature. High-temperature treatments (260 °C) produced a continuous Pd film mostly absent of organic materials and with no Pd discontinuities, resulting in a decrease in current as expected for a typical bulk Pd film. Low-temperature treatments led to partial monolayer desorption and a film with a considerable number of discontinuities (or break junctions). In the presence of H_2, the Pd expands in volume, reducing the number of discontinuities and increasing the conductivity. Despite the inconvenience of performing pretreatments to the film, all the sensors reported were sensitive to H_2 well below the explosive limit of 4%.

Hanwell et al. prepared Langmuir–Schaeffer 2D Au films comprised of C12S, C6S, and 4-methylbenzenethiol MPCs for chemiresistive sensing of NO_2 gas.[52] C12S Au MPCs displayed a high film resistance above the limit of the instrument. The authors observed that C6S- and 4-methylbenzenethiol-coated nanoparticle films were responsive

to small concentrations of NO_2 indicated by an increase in conductivity. The film of C6S Au MPCs displayed reversible, reproducible, and stable current changes in the presence of 1 ppm NO_2 at room temperature. The lowest detection limit achieved was below 0.5 ppm. The authors speculated that the increase in conductivity may be produced by changes in permittivity when gas molecules partition into the film.

7.1.2. Alkylamine-Coated Nanoparticles

In order to improve the reactivity between organic-modified Pd nanoparticles and H_2 and avoid the inconvenient pretreatment steps described for C6S Pd MPCs (ozone or temperature), our group synthesized various amine-coated Pd MPCs, including those coated with octylamines ($C8NH_2$), dodecylamines ($C12NH_2$), and hexa- and octadecylamines ($C16–C18NH_2$).[55] The films were immediately reactive and sensitive towards the presence of H_2 gas at various concentrations after some conditioning steps. All the films were conditioned with saturated H_2 before the sensors became fully operational. Films of $C8NH_2$ and $C12NH_2$ Pd MPCs displayed large 3–4 order-of-magnitude increases in current in the presence of 100% H_2 during conditioning. Once the baseline reached a stable 10^{-4}–10^{-3} A current level, the films responded by exhibiting a decrease in current in the presence of H_2 as expected for bulk, highly conductive Pd films. Films of $C12NH_2$ MPCs displayed a current initially around the 10^{-8} A level and responded to H_2 with an increase in current. The low conductivity suggests that the film contained well-separated Pd nanoparticles and we attributed the increase in current to a decrease in the edge-to-edge separation upon volume increase of the Pd metal in the film as it formed PdH_x. The conductivity of this film eventually increased to the 10^{-4} or 10^{-3} A level over time and showed the behavior of a bulk Pd film. We observed that the kinetics of H_2 reactivity decreased as the chainlength increased, consistent with a blocking effect that the organic material may impose. For instance, $C16–18NH_2$ Pd MPCs displayed no increase in current after 100% H_2 for several minutes. The best films of alkylamine-coated Pd MPCs generally detected H_2 down to the 800 ppm level.

7.1.3. Mixed Alkylamine- and Organomercaptan-Coated Nanoparticles

More recently our group synthesized a mixed monolayer of octylamine ($C8NH_2$)- and hexanethiol (C6S)-coated Pd nanoparticles by performing liquid-phase place exchange of the amines with thiols in a controlled manner.[98] The Pd MPCs are in the form of $Pd_{919}(C6S)_{192}$ or $Pd_{919}(C8NH_2)_{177-x}(C6S)_x$, where x was varied to be 0, 3, 10, 16, 32, or 81 by the synthesis of pure $C8NH_2$ Pd MPCs and subsequent liquid-phase place exchange with a varied amount of C6SH. Amine-coated MPCs as discussed in the previous section readily reacted with H_2 gas leading to large morphology changes and long activation times while thiol-coated MPCs reacted minimally and irreversibly. The optimal number of RSH ligands for this study was in the range of x = 32–81, which exhibited high reactivity to H_2, little morphology changes or aggregation, and stable, reversible responses to H_2 concentrations between 9.0 and 0.3%,

7.1.4. Surfactant-Coated Nanoparticles

Our group also investigated chemiresistive H_2 sensing with tetraoctylammonium bromide (TOABr)-stabilized Pd nanoparticles.[55] We synthesized these Pd nanoparticles by borohydride reduction of $PdCl_4^{2-}$ in the presence of the TOABr surfactant in toluene. The TOABr acts as a stabilizer, rather than as a protective monolayer, since it is in large excess in solution beyond the amount needed for one monolayer. These nanoparticles would not be stable with only a single monolayer coating of TOABr because of its weak affinity for Pd relative to thiolates. As-prepared films showed low baseline currents due to the large excess of TOABr in the film after drop-cast deposition. However, the films were readily sensitive to the presence of H_2 down to the concentration of 0.11% (1100 ppm) with no pretreatment or conditioning steps. The film responded to H_2 by an increase in conductivity, but the sensing mechanism is not well understood at this time.

7.1.5. DNA-Coated Nanoparticles

Hatakeyama et al. recently synthesized bare Pd nanoparticles and Pd nanoparticles embedded in DNA by using a combination of metallization and DNA compaction.[51] Morphology changes were due to variations in the DNA strand conformation when the backbone cations complex with the Pd ions, causing a transition from a coil to a compact structure. These hybrid films were dried on top of glass in between a pair of electrodes to compare their chemiresistive sensing properties in the presence of low concentrations of H_2. Bare Pd was obtained by reducing Pd^{2+} to Pd^0 with ascorbic acid while DNA-compacted Pd clusters were synthesized using ascorbic acid and $NaBH_4$. **Figure 13**A shows a chemiresistive response of bare Pd (citrate coated) and DNA-protected Pd nanoparticles upon exposure to 0.1 and 1% H_2 concentration. The bare Pd films were highly conductive and kept increasing in current irreversibly when exposed to 1% H_2 (top figure). In contrast, the DNA-coated Pd nanoparticles show low, stable, and reversible current responses to 1% and 0.1% (small response peaks) H_2 concentration. The figure clearly shows that films of DNA-coated Pd clusters readily react with H_2 and are capable of detecting down to 1000 ppm H_2. The authors attributed the increase in current to volume expansion caused by the formation of PdH_x and a shortened PdH_x–PdH_x distance. DNA-coated Pd clusters synthesized using borohydride were less sensitive to H_2 probably due to the formation of a less homogenous film as compared to those Pd clusters reduced with ascorbic acid. The authors suggest that film homogeneity plays a role in the volume contraction–expansion behavior and accordingly affects sensitivity.

7.1.6. Other Drop-Coated Metal and Alloy Nanoparticle Films

We synthesized TOABr-protected PdAg and amine-coated PdAg and PdAu alloy MPCs of various chainlength (C8, C12, C14, C16) for sensing H_2 gas.[55] Films of $C8NH_2$ PdAg MPCs (10:1 Pd:Ag ratio) exhibited high sensitivity, a low limit of detection, excellent stability, fast response, and short conditioning time to reach stable sensing behavior as shown in Figure 13B (top-plot). Films of $C8NH_2$ PdAu

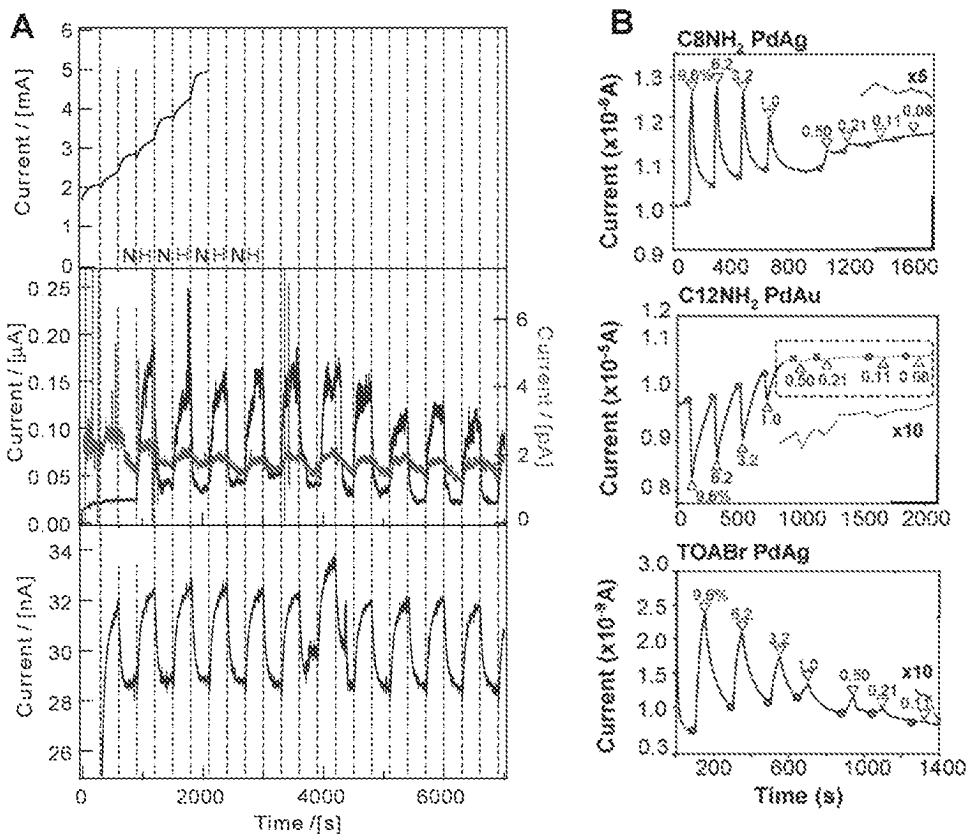

Figure 13. A) Current response for Pd nanoparticles synthesized with ascorbic acid and without DNA (top-left panel), with ascorbic acid and DNA (middle-left panel), and with $NaBH_4$ and DNA (bottom-left panel) exposed to H_2 from 1% to 0.1% (small response peaks at the middle-left figure) concentration and B) current–time plots for $C8NH_2$ PdAg (top-right panel), $C12NH_2$ PdAu (middle-right panel), and TOABr-coated PdAg (bottom-right panel) nanoparticle films exposed to H_2 concentrations as noted. Reproduced with permission.[A][51][B][55]

alloy MPCs showed a very large and irreversible 7 order-of-magnitude increase in current during conditioning in H_2 and were not useful for sensing (not shown here). Films comprised of $C8NH_2$- and $C12NH_2$-coated PdAg and PdAu alloy MPCs reacted with 100% H_2 leading initially to an irreversible increase in current and then showing stable, reversible changes in the presence of H_2 concentrations from 9.6 to 0.08% as indicated in Figure 13B (middle-plot). Comparing films of $C8NH_2$ PdAg MPCs with those of $C8NH_2$ Pd MPCs, the presence of Ag led to lower currents (10^{-8}–10^{-7} A) due to greater stability, a current increase in the presence of H_2, and a slightly higher percent response. Interestingly, less than 10% Ag in the nanoparticle led to very low currents (10^{-8} A) after conditioning in 100% H_2, whereas films of $C8NH_2$ Pd (no Ag) exhibited currents on the 10^{-4} A level after conditioning in 100% H_2. Fourier-transform infrared (FT-IR) and AFM data showed that the latter films exhibit a greater loss of $C8NH_2$ ligands and greater change in film morphology after conditioning. The small amount of Ag clearly improved $C8NH_2$ binding, which prevented large film morphology changes or nanoparticle aggregation. This led to the lower currents. Importantly, while $C8NH_2$ binds more tightly and remains on the MPCs, the H_2 still readily reacts with the MPCs and causes a conductivity change. Films of TOABr-coated PdAg alloy nanoparticles readily reacted with H_2, leading to reversible current increases from 0.11 to 9.6% H_2 with no pretreatment or conditioning, as shown in Figure 13B (bottom-plot). These experiments reveal the importance of the metal and coating compositions and the benefits of alloying.

7.2. Chemically-Linked Films of Metal Nanoparticles

Joseph et al.[47] prepared films of $C12NH_2$ Pt and Au MPCs via layer-by-layer self assembly with 1,9-nonanedithiol and exposed the films to ammonia (NH_3), carbon monoxide (CO) gas, and other vapors as discussed in Section 6. They noticed that film resistance increased in the presence of the gases and that gas analytes bind stronger to the metal core relative to vapors, based on the curvature of the response isotherms and the three orders of magnitude longer residence time of the analyte in the film. This evidence led the researchers to conclude that gas analytes preferentially bind to vacant sites on the metal core while vapor analytes interact more with the organic material in the film, consistent with the swelling mechanism and increase in film resistance. However, the increase in resistance observed for NH_3 and CO gas analytes still remains unclear.

Murray and co-workers studied electron transport and response to CO_2 as a function of the mixed valence state of small phenyl ethanethiol (–SC2Ph)– and poly(ethylene glycol)-coated Au_{38} MPCs.[21] Mixed valent films of Au_{38} MPCs

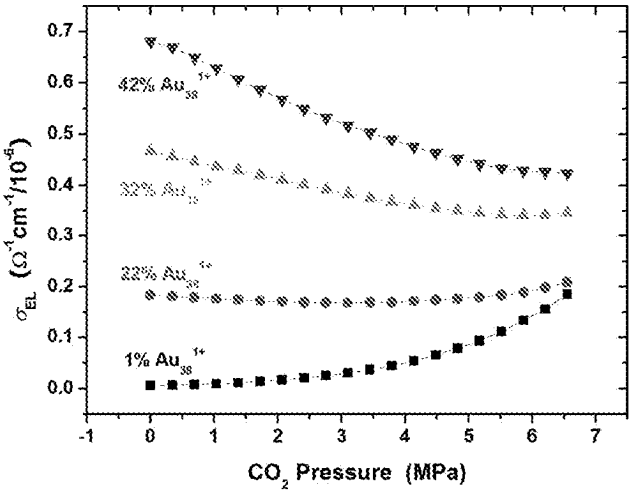

Figure 14. Conductivity (σ_{EL}) dependence on CO_2 pressure for mixed-valent Au_{38} nanoparticle films. Reproduced with permission.[21]

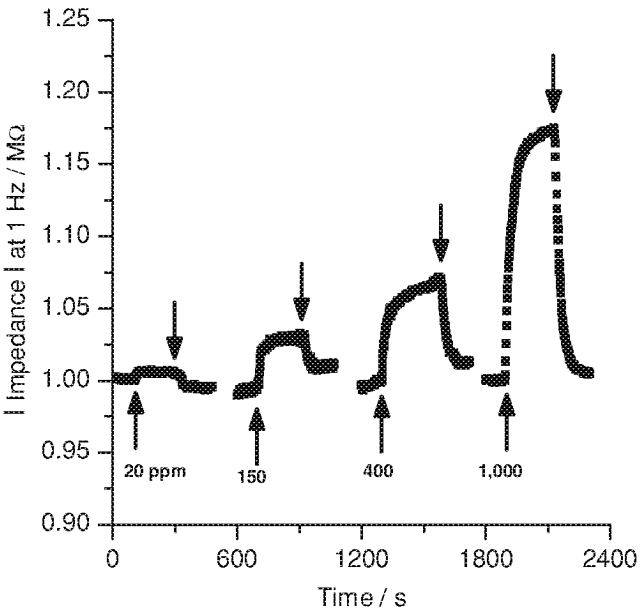

Figure 15. Impedance measurements for a film comprised of C6S Au MPCs immersed in KCl solution and exposed to dichloromethane dissolved in the electrolyte solution at the indicated concentrations. Reproduced with permission.[79]

were obtained by bulk electrolysis of solutions containing the nanoparticles. By controlling the potential, they controlled the ratio of Au_{38}^{0} and Au_{38}^{+1} and then assembled them as films by drop-cast deposition onto an IDA of electrodes without the nanoparticles losing their charge states.[99] The authors then exposed the films to an increasing concentration of CO_2 as shown in **Figure 14**. The data show that the baseline conductivity in the absence of CO_2 increases with increasing percent valency from 1% to 42%, consistent with the authors' previous work.[21] Also, as the CO_2 pressure increased, the conductivity of the film increased for those with a low percentage of +1 valence and decreased for those with a higher percentage of +1 valence nanoparticles. Interestingly, the conductivity of films of 22% Au_{38}^{+1} slightly decreased with increasing CO_2, reached a plateau, and then finally increased. Based on the results, the authors proposed that there is a tradeoff between local thermal motions leading to a conductivity increase and constraint in the local mobility of the nanoparticles leading to a conductivity decrease. The latter is due to electrostatic interactions between +1 charged MPCs and their counterions.

8. Chemiresistive Sensing in Liquids

8.1. Sensing Organics in Water

Raguse et al. prepared films of C6S Au MPCs for detecting organic analyte dissolved in ionically conductive electrolyte solution.[79] In order to measure the conductivity changes, or impedance, through the film of MPCs and not through the electrolyte solution, the film was miniaturized by inkjet printing of the Au nanoparticles onto photolithographically patterned microelectrodes. MPCs assembled into films can be considered as a circuit comprised of capacitors and resistors and represented in terms of impedance (Z) through the following equation:[100]

$$Z^{-1} = \left(\frac{2}{i\omega C_{dl}}\right)^{-1} + R_s^{-1} + R_f^{-1} \quad (9)$$

where i is the imaginary unit, ω the angular frequency, C_{dl} the double-layer capacitance, R_s the solution resistance, and R_f the nanoparticle film resistance. According to the above equation, inverse impedance is related to the sum of the inverse of film resistance, electrolyte resistance, and double layer capacitance, where the latter term depends on the distance between the particles, the material between the metallic cores, and the geometry of the electrode. If the operating frequency, film size, and electrode gap are minimized, then the first two terms in Equation 9 become negligible and the impedance becomes equal to the film resistance (R_f). **Figure 15** shows an impedance–time plot for a film of C6S MPCs exposed to 20, 150, 400, and 1000 ppm dichloromethane dissolved in 1 M KCl solution. The Figure indicates that the film impedance increased relatively fast in the presence of dichloromethane, changed slowly to reach equilibrium, and then returned immediately to the baseline in the absence of the analyte. The authors demonstrated that C6S Au MPC films detected down to 0.1 ppm of toluene, which is below the limit established by the World Health Organization. The authors concluded that C6S Au MPC films have a higher affinity for nonpolar vapors than polar vapors as indicated by the sensitivity response trend of toluene > dichloromethane > ethanol.

Following this work, Chow et al. compared the chemiresistive response of inkjet-printed films of different size and shape to small organic molecules, such as toluene, dichloromethane, and ethanol dissolved in electrolyte solution.[100] They demonstrated that the film uniformity can be improved by inking the film of MPCs from a mixture of *N*-methyl-2-pyrrolidone and water in a two-solvent system. The response time and sensitivity of coffee-ring and flat films were similar in the presence of organic analytes, indicating that the shape

and thickness had no effect on the sensing performance. However, when both films were exposed to a more hydrophobic analyte (octane), the response time for flat films was five times faster than the coffee-ring, showing that there is a relationship between the kinetics and the film morphology/thickness.

More recently, the same group compared hydrophobic and hydrophilic chemiresistive films to nonpolar and polar analytes.[54] They found that films of MPCs coated with a mixed monolayer of hydroxyl-hexanethiolate and hexanethiolate and 4-mercaptophenol and hexanethiolate readily responded to polar and nonpolar analytes in aqueous solution. Consistent with the film–vapor affinity, the sensitivity to polar liquids (i.e., EtOH) was best when sensing with films of MPCs coated with hydroxyl-hexanethiolate. These films exhibited a ≈3 fold response improvement in the presence of ethanol as compared to conventional C6S Au MPCs.[54,101] This work demonstrated an elegant and simple method for sensing organic analytes incorporated into a conductive solution and the possibility of fabricating multi-sensor arrays for building an 'electronic tongue' by inkjet-printing of nanoparticles with different functionalities.

8.2. Sensing with Individual Nanoparticles

Feldheim and co-workers[56] conducted STM studies on C8S- and galvinol (Gal)-coated Au nanoparticles in water at different pH values. They observed Coulomb staircase behavior for C8S Au and Gal Au nanoparticles exposed to pH values ranging from 5 to 12. Individual C8S Au clusters did not show significant changes in Coulomb staircase at different pH values relative to galvinol which at pH ≈10 oxidized to galvinoxide. The most prominent change for galvinol was observed at pH 12, where the Gal–Au cluster was deprotonated to the form of galvinoxide anion. This leads to an increase in capacitance and an increase in negative charge around the cluster surface observed by a potential shift. The authors concluded that since there were no changes in Coulomb staircase for C8S Au MPCs as opposed to Gal–Au MPCs, there must be pH-gated SET which controls the electron tunneling attributes by subtle changes in the nanoparticle environment. This experiment elegantly demonstrates the importance of the cluster environment on the ability to study SET events in chemically modified metal nanoparticles.

Schiffrin and co-workers reported the use of polymethylene-coated Au nanoparticles that carry a central, reversibly reducible bipyridinium molecule that changes from ON to OFF when adding or withdrawing an electron in SET experiments.[57] Polymethylene stabilizes the cluster while bipyridinium serves as a redox molecule that is oxidized and reduced by controlling the substrate-to-solution potential. **Figure 16** shows a nanoscopic electronic switch comprised of a single MPC attached

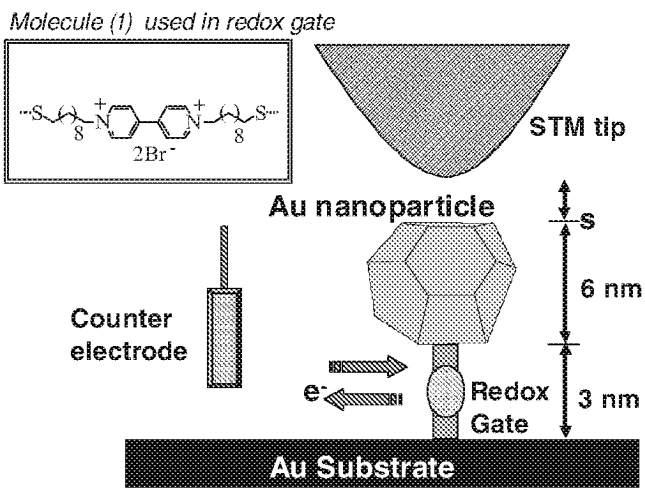

Figure 16. Schematic representation of the nanoscale device indicating the redox states of the bipyridinium molecule. Reproduced with permission.[57]

to the substrate via thiol chemistry. The figure shows schematically the redox states of the bipyridinium molecule indicating an 'OFF state' when the molecule is oxidized and 'ON state' when the molecule is reduced. The authors created molecular switches by using a redox-switchable device that can store bits and detect single molecules or chemical reactions.[102] This work represents a nice example of using the electronic properties of a single nanoparticle through sensing changes in the redox state of a molecule located between tip–nanoparticle and substrate.

8.3. Biosensing with Metal Nanoparticles

8.3.1. DNA Sensing

Mirkin and co-workers utilized the electronic properties of Au nanoparticles in order to detect oligonucleotides as shown in **Figure 17**.[58] In their experiment, a microelectrode chip with an electrode gap size of 20 μm was first modified with the oligonucleotide capture strands in between the microelectrode gap. The capture strand is half complementary

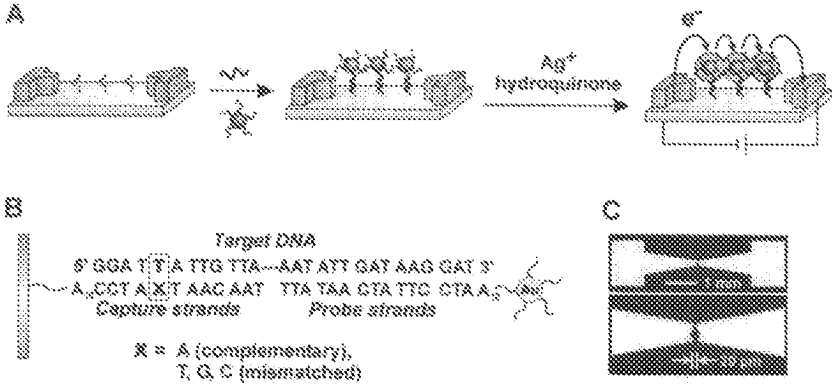

Figure 17. A) Schematic representation of the experimental steps for electrical detection of DNA, B) capture target and probe DNA, and C) an optical microscope image of the electrode used. Reproduced with permission.[58]

with the target DNA of interest. The authors functionalized Au nanoparticles with probe oligonucleotides that are complementary to the other half of the target DNA. When the microelectrode, target DNA, and Au nanoparticles are brought together in a solution, the target DNA will cause the Au nanoparticles to bind to the microelectrode chip in the gap between the electrodes by hybridizing with both the capture and probe oligonucleotides on the chip surface and Au nanoparticles, respectively. This does not directly lead to a conductance pathway between the electrodes since the Au nanoparticles are not well-connected. For this reason, the film was treated with $AgNO_3$ (Ag^+) and hydroquinone as a conductivity enhancer caused by the growth of Ag^0 on the surface of the attached Au nanoparticles. The deposition of Ag on the Au nanoparticles leads to a conductive pathway and measurable signals. The authors demonstrated that in the absence of DNA, there was no conductivity change even after 40 min of silver enhancement. Through this method, Mirkin's group was able to detect target DNA down to 500 femtomolar without the need for a thermal-stringency wash. They were also able to discriminate the complementary target DNA from three different DNA that each contained a single-base mismatch.

Nagaoka and co-workers[72] studied the resistance change of probe DNA-functionalized 80 nm-diameter Au nanoparticles assembled by dithiol cross-linking across an electrode gap following exposure to mismatched and complementary target DNA. They formed a conductive film by repeated dipping cycles of decanedithiol and Au nanoparticles (see Figure 2B) with further functionalization of the Au nanoparticles with single strand probe DNA (ssDNA). The presence of the complementary target DNA hybridization on the film led to a direct increase in the electrical conduction through the Au nanoparticle assembly without the need for an enhancement step. The results show that the presence of mismatched and complementary base pairs (bp) decreased the film resistance by different amounts. The researchers could readily distinguish between the fully complementary target oligonucleotide and oligonucleotides with one base pair mismatch because the former showed a larger decrease in resistance. The larger decrease in resistance was attributed to π overlapping between adjacent base pairs, which facilitated the electron transport via delocalized electrons present in hybridized DNA. A later study from the same group showed that the sensitivity could be enhanced by precisely controlling the distance between Au nanoparticles by using a 1.3 nm decanedithiol linker.[74,103] They observed a remarkable conductivity difference between the 1-base-pair mismatch and complementary DNA sequence and no apparent difference between 4- and 11-base-pair mismatched DNA.[74]

Fang et al.[59] fabricated a biosensor for the detection of a 22-mer oligonucleotide by using aggregated films of 3-mercaptopropionic acid (MPA)-coated Au nanoparticles. The gap of SiO_x between the Au microelectrodes was functionalized with peptide nucleic acid (PNA) which acted as a capture site for the DNA. The inorganic linker Zr^{4+} was used for both enhancing the conductivity of the film by forming nanoparticle aggregates and attaching complementary DNA via electrostatic interaction between Zr^{4+} with the MPA and Zr^{4+} with the negatively charged phosphate of DNA, respectively. The calibration curve showed no conductivity for the control (no DNA hybridization) and a linear relationship between the target DNA and one- and two-base-pair mismatch DNA with the following conductivity trend of target DNA > 1-base-pair mismatch DNA > 2-base-pair mismatch DNA. The authors concluded that the target DNA concentration is crucial for attaching more nanoparticles into the gap and forming more conductive pathways to improve conductivity. In this work, the lowest detection limit achieved was 5×10^{-14} M.

9. Summary and Future Directions of the Field

There are clearly several benefits of using chemically modified metallic nanoparticles in chemiresistive sensing devices. First, a number of strategies exist that allow the controlled synthesis of nanoparticles with different metal compositions and stabilizers, including self-assembled monolayers, ions, surfactants, polymers, or biomolecules for sensing molecules in the gas or liquid phase. The use of various functional groups or specific metals often allows one to selectively detect a specific analyte of interest. Alternatively, sensor arrays constructed from a wide variety of functional groups allows one to distinguish different analytes through principle-component analysis. Second, there are a number of simple, low-cost methods available for fabricating electrode devices and assembling the nanoparticles into 2D or 3D arrangements across electrode contacts. Photolithography combined with ink-jet printing is particularly promising for fabricating a large number of devices in a low cost, large-scale, parallel manner.[78,100] The amount of material needed is small, which leads to a low cost even when expensive metals like Au, Pd, and Pt are used. Third, the devices are electronic and therefore amenable to miniaturization, which usually leads to rapid measurements in the field as opposed to sending samples to a lab for analysis. Miniaturization carries the added benefits of low cost, low waste, and low power consumption as well. Finally, chemiresistors have proven to be quite sensitive, fast, and reproducible for several applications, although improvements are always needed in these areas. A summary of vapor, gas, and liquid sensing and future challenges and directions of the field follows.

By far the most common application for chemiresistive sensing with metal nanoparticles is for the detection of VOCs.[27] There are several factors that control the sensing attributes, including particle size,[40] film size,[41,78] type of stabilizer,[38] type of metal,[47] and even metal valence state.[21] Monolayer-protected clusters (MPCs) are the most common type of nanoparticles used to detect VOCs. Researchers usually employ 3D films of organomercaptan SAM-coated Au MPCs in these studies.[27,49] The film conductivity is based on the well-established electron hopping mechanism,[81] where the edge-to-edge distance and the dielectric properties of the environment are the major factors. A change in one or both of these two variables, or even the electron tunneling coefficient, in the presence of the analyte can alter the electronic properties, providing a signal for the analyte of interest. It is not always well-known which factor dominates, but in the

case where the vapor analyte causes swelling of the nanoparticle film and a resistance increase due to an increase in the metal edge-to-edge distance, it has been shown that the signal increases 1) when the polarity of the nanoparticle coating matches well with the polarity of the vapor analyte,[28] 2) when the film is highly flexible,[41] which is achieved by minimizing cross-linking between metal nanoparticles or by increasing the chainlength of alkanethiolate-coated metal nanoparticles, 3) when there are more sites for analyte adsorption in the film,[30] and 4) as the room temperature analyte vapor pressure decreases.[33] The size of the nanoparticles can play a role,[40] although it is not very clear, and the size of the 3D film down to the microscale does not have a significant effect on the sensing characteristics.[41,78] The metal composition of the nanoparticles apparently plays an important, but poorly understood role since researchers observed different sensing behaviors for Pt[47] and AuAg[38] alloys as compared to pure Au nanoparticles.[39,96] The film thickness (or coverage) affects the sensing mechanism. When it is below the percolation threshold, a resistance decrease occurs due to vapor-induced swelling and the connection of island films within the partial layer to create conductive pathways.[96] Once a certain thickness is reached, however, the more common vapor-induced swelling and resistance increase occurs instead and the sensitivity does not change much,[39] although the signal-to-noise may improve with thicker films and response time increases with smaller, thinner films.[34] The sensing mechanism becomes dominated by the permittivity difference between the analyte and medium when the film is rigidly linked.[94] Metal nanoparticles with highly conductive and rigid coatings exhibit very poor sensitivity to vapor-phase analytes.[94] The selectivity for a specific analyte is generally poor when sensing VOCs. The electronic response of nanoparticles with nonpolar coatings is larger for nonpolar vapors compared to polar vapors, but not selective enough to determine the identity and quantify the amount of each VOC in a complex mixture. In that case, it is necessary to fabricate sensor arrays comprised of nanoparticle films with various coatings, including surfactants[38] and other nontraditional coatings,[48] and employ pattern recognition to determine the analyte identity.[34,39] When coupled with gas chromatography (GC),[31] this can be a powerful method for separating, identifying, and quantifying a complex mixture of vapor analytes, although the use of GC adds to the cost and device bulkiness. The detection limit of devices are generally in the low ppm range, although lower limits can be reached by preconcentration strategies.[31]

There are far fewer examples of chemiresistive gas sensors employing chemically modified metal nanoparticles. The most popular example involves hydrogen sensing with Pd and Pd-containing films of metal nanoparticles.[55] Here, the electron hopping equation is still relevant, but the mechanism is very different compared to the detection of VOCs since the gas analyte generally interacts directly with the metal portion of the nanoparticles instead of the organic monolayer. The organic stabilizer controls the initial electronic properties of the film, but the gas–metal interaction is responsible for the conductivity change. In that case, it is important to utilize a stabilizer that prevents metal nanoparticle aggregation and size, shape, or morphology changes, but allows the gas molecules to directly ineract with the metal.[98] Strongly coordinated ligands, such as thiols on Pd, are typically detrimental since they prevent the metal–gas interactions necessary to measure electronic changes. Ligands not bound strongly enough may lead to nanoparticle size and shape changes or irreversible aggregation of the nanoparticles, which could be equally detrimental. In our studies, we found that PdAg alloy nanoparticles coated with octylamine ligands,[55] pure Pd nanoparticles coated with mixed hexanethiol and octylamine ligands,[98] and tetraoctylammonium bromide (TOABr)-coated Pd nanoparticles[55] were capable of stabilizing the nanoparticles, but also allowed reactivity with H_2 gas and detection well below the explosive limit. Others have used Pt nanoparticles for CO and NH_3 sensing,[47] Au MPCs for NO_2 sensing,[52] and mixed valent films of Au_{38} MPCs for the detection of CO_2 gas.[21] The selectivity of metal nanoparticles for chemiresistive gas sensing depends on the system. For example, Pd metal is highly selective towards H_2 with few interferents, but this is not the case for all systems and the metal–gas or monolayer–gas interaction is often poorly understood.

The detection of analytes in liquid are more common compared to gas sensing, but less common compared to the detection of VOCs. The examples provided here include the detection of organics dissolved in aqueous electrolyte[79] and the detection of biomolecules, such as DNA.[58,76] In the case of detecting organics, such as toluene and dichloromethane, the researchers detected the organics at the low 0.1 ppm level in some cases and found that the film morphology was not important.[100] With a more hydrophobic analyte (octane), the response time for flat films was five times faster compared to the coffee-ring films, showing that there is a relationship between the kinetics and the film morphology/thickness for more hydrophobic analytes.[100] The selectivity of these films is similar to the films for sensing VOCs. They will generally respond to all organics that can nonspecifically partition into the films. A larger response will occur for analytes that match the polarity of the monolayer coating, but it is not highly specific. Sensor arrays and analyte separation would be beneficial and the technique would work well in less complex solutions. Researchers have been able to distinguish between a fully complementary target oligonucleotide and oligonucleotides with one base-pair mismatch in aqueous solution by observing changes in film resistance upon direct hydridization of the target ss-DNA and the complementary probe strand bound to the nanoparticle film[59] or by indirect metallization of metal nanoparticles that assembled between a pair of electrodes upon hybridization of target and probe DNA strands attached to the electrode gap and metal nanoparticles.[58] These films can detect femtomolar quanitites of DNA and are highly specific due to the highly specific binding of the target and complementary probe DNA.

Chemiresistors comprised of metal nanoparticles have potential for use in the industrial sector. The benefits have been described in terms of simplicity, low cost, sensitivity, detection limit, miniaturization, and reproducibility, but several challenges exist. One main problem is selectivity. It would be a tremendous achievement to completely analyze a complex mixture (identity and quantity) with a small, handheld chemiresistive device without the use of a prior

separation by GC or even detect one analyte of interest in the presence of a complex mixture of interferents. There is a need for further exploration of other metal nanoparticle coatings that could impart greater selectivity, which could include metal–ligand complexes, various polymers or polyelectrolytes, surfactants, molecular imprinted films, or aptamers as some examples. The vast majority of studies have dealt with simple alkanethiols and other functionalized organomercaptans, leaving great room for further exploration. Another issue is long term reproducibility, stability, and durability. The nanoscale metals, alkanethiolate SAMs, or other types of stabilizers are often susceptible to air oxidation over time, leading to baseline drift, unpredictable response, or eventual loss in function.[104,105] Poor thermal stability could be an issue in certain environments with SAMs and nanoscale metals. Most of the studies to date explore the response of newly fabricated devices and do not address long term stability and use under a variety of environments, especially those that are harsh. Optimized miniaturization and integration of the metallic nanoparticles onto the sensing device is a technical challenge that will also need to be addressed in future studies. An improvement in the sensitivity and detection limits below the low ppm level will be required for many applications. Researchers need to push into the low ppb or even ppt range without the need for preconcentration to compete with other technologies and expand applications.

Lower detection limits can hopefully be achieved through fundamental studies and a better understanding of the relative contributions of the change in nanoparticle-nanoparticle distance, permittivity, and β_d on the sensing response as a function of the metal composition, ligand composition, film thickness, film size, and type of organization (3D, 2D, or 1D). Future studies will be needed to obtain detailed structural, chemical composition, and electronic information during sensing to better understand the mechanism in order to rationally design films with improved sensing attributes. Improvements in the surrounding receptor ligands or device miniaturization could potentially improve the detection limits. There have been no detailed studies on the effects of nanoparticle composition, nanoparticle shape, and film deposition techniques on the sensing attributes. It would be interesting to compare the chemiresistive properties of 3D, 2D, and 1D assemblies. STM studies of single nanoparticles show high sensitivity to their environment, but researchers have not yet been able to easily fabricate single-nanoparticle or 1D-nanoparticle array devices. More information is needed on the effect of nanoparicle size on the chemiresistive sensing properties, especially for very small metal nanoparticles, where they develop a bandgap.[106] Progress in these areas could lead to detection limits potentially down to the single-molecule level someday.

Acknowledgements

The authors gratefully acknowledge the National Science Foundation (CHE-0518561 and CHE-0848883) and the Kentucky Science and Engineering Foundation for financial support of their research. F.J.I. acknowledges Agencia Nacional de Promoción Científica y Tecnológica for the Program PRH-74 which has greatly helped to performed research back in Argentina. F.J.I. also gratefully acknowledges Dr. Roberto C. Salvarezza the director of Instituto de Investigaciones de Fisicoquímicas Teóricas y Aplicadas (INIFTA), for his help with repatriation issues. We acknowledge the manuscript reviewers, expecially Reviewer 1, for taking time to provide extensive, detailed comments and suggestions that led to a greatly improved manuscript.

[1] R. C. Hughes, W. K. Schubert, *J. Apply. Phys.* **1992**, *71*, 542
[2] M. E. Franke, T. J. Koplin, U. Simon, *Small* **2006**, *2*, 36.
[3] K. J. Albert, N. S. Lewis, C. L. Schauer, G. A. Sotzing, S. E. Stitzel, T. P. Vaid, D. R. Walt, *Chem. Rev.* **2000**, *100*, 2595.
[4] R. Dutta, E. L. Hines, J. W. Gardner, K. R. Kashwan, M. Bhuyan, *Sens. Actuators B* **2003**, *94*, 228.
[5] H. Yan, H. Choe, S. S. Nam, Y. Hu, S. Das, J. F. Klemic, J. C. Ellenbogen, C. M. Lieber, *Nature* **2010**, *470*, 240.
[6] B. J. Hollidey, T. B. Stanford, T. M. Swager, *Chem. Mater.* **2006**, *18*, 5649.
[7] N. S. Lewis, *Acc. Chem. Res.* **2004**, *37*, 663.
[8] F. A. Lewis, *The Palladium/Hydrogen System*, Academic Press Inc., London **1967**.
[9] L. Han, X. Shi, W. Wu, F. L. Kirk, J. Luo, L. Wang, D. Mott, L. Cousineau, S. I.-I. Lim, S. Lu, C.-J. Zhong, *Sens. Actuators B* **2005**, *106*, 431.
[10] R. M. Crooks, A. J. Ricco, *Acc. Chem. Res.* **1998**, *31*, 219.
[11] J. W. Grate, *Chem. Rev.* **2000**, *100*, 2627.
[12] J. Yinon, *J. Anal. Chem.* **2003**, 99A.
[13] D. J. Strike, M. G. H. Meijerink, M. Koudelka-Hep, *Fresenius J. Anal. Chem.* **1999**, *364*, 499.
[14] A. K. Pavlou, A. P. F. Turner, *Clin. Chem. Lab. Med.* **2000**, *38*, 99.
[15] R. Dasari, F. P. Zamborini, *J. Am. Chem. Soc.* **2008**, *130*, 16138.
[16] I. Heller, A.M. Janssens, J. Mannik, E. D. Minot, S. G. Lemay, C. Dekker, *Nano Lett.* **2008**, *8*, 591.
[17] D. B. Wolfe, J. C. Love, K. E. Paul, M. L. Chavinyc, G. M. Whitesides, *Apply. Phys. Lett.* **2002**, *80*, 2222.
[18] G. Sberveglieri, C. Faglia, C. Perego, P. Nelli, R. Marks, N. T. Virgili, C. Taliani, R. Zamboni, *Synthetic Met.* **1996**, *77*, 273.
[19] M. Myers, J. Cooper, B. Pejcic, M. Baker, B. Raguse, *Sens. Actuators B* **2011**, *155*, 154.
[20] Y. Dan, Y. Lu, N. J. Kybert, Z. Luo, A. T. Charlie Johnson, *Nano Lett.* **2009**, *9*, 1472.
[21] J.-P. Choi, M. M. Coble, M. R. Branham, J. M. DeSimone, R. W. Murray, *J. Phys. Chem. C* **2007**, *111*, 3778.
[22] A. Zabet-Khosousi, A. Dhirani, *Chem. Rev.* **2008**, *108*, 4072.
[23] R. W. Murray, *Chem. Rev.* **2008**, *108*, 2688.
[24] H. Haick, *J. Phys. D: Appl. Phys.* **2007**, *40*, 7173.
[25] M.-C. Daniel, D. Astruc, *Chem. Rev.* **2004**, *104*, 293.
[26] E. Boisselier, D. Astruc, *Chem. Soc. Rev.* **2009**, *38*, 1759.
[27] H. Wohltjen, A. W. Snow, *Anal. Chem.* **1998**, *70*, 2856.
[28] H.-L. Zhang, S. D. Evans, J. R. Henderson, R. E. Miles, T.-H. Shen, *Nanotechnology* **2002**, *13*, 439.
[29] E. E. Foos, A. W. Snow, M. E. Twigg, M. G. Ancona, *Chem. Mater.* **2002**, *14*, 2401.
[30] H. Ahn, A. Chandekar, B. Kang, C. Sung, J. E. Whitten, *Chem. Mater.* **2004**, *16*, 3274.
[31] Q.-Y. Cai, E. T. Zellers, *Anal. Chem.* **2002**, *74*, 3533.
[32] N. Garg, A. Mohanty, N. Lazarus, L. Schultz, T. R. Rozzi, S. Santhanam, L. Weiss, J. L. Snyder, G. K. Fedder, R. Jin, *Nanotechnology* **2010**, *21*, 405501.
[33] W. H. Steinecker, M. P. Rowe, E. T. Zellers, *Anal. Chem.* **2007**, *79*, 4977.

[34] E. Covington, F. I. Bohrer, C. Xu, E. T. Zellers, C. Kurdak, *Lab Chip* **2010**, *10*, 3058.
[35] E. Dovgolevsky, G. Konvalina, U. Tisch, H. Haick, *J. Phys. Chem. C* **2010**, *114*, 14042.
[36] J. K. Kim, Y. S. Yang, S. C. Ha, S. M. Cho, Y. S. Kim, H. Y. Kim, H. Yang, Y. T. Kim, *Sens. Actuators B* **2005**, *106*, 189.
[37] S. M. Briglin, T. Gao, N. S. Lewis, *Langmuir* **2004**, *20*, 299.
[38] F. J. Ibañez, F. P. Zamborini, *ACS Nano* **2008**, *2*, 1543.
[39] L. Han, D. R. Daniel, M. M. Maye, C.-J. Zhong, *Anal. Chem.* **2001**, *73*, 4441.
[40] L.-S. Wang, K. Xiajing, N. N. Karuiki, M. Schadt, G. R. Wang, Q. Rendeng, J. Choi, J. Luo, S. Lu, C.-J. Zhong, *J. Am. Chem. Soc.* **2007**, *129*, 2161.
[41] F. J. Ibañez, U. Growrishetty, M. M. Crain, K. M. Walsh, F. P. Zamborini, *Anal. Chem.* **2006**, *78*, 753.
[42] M. Toda, Y. Joseph, R. Berger, *J. Phys. Chem. C* **2010**, *114*, 2012.
[43] T. Vossmeyer, B. Guse, I. Besnard, R. E. Bauer, K. Mullen, A. Yasuda, *Adv. Mater.* **2002**, *14*, 238.
[44] F. P. Zamborini, M. C. Leopold, J. F. Hicks, P. J. Kulesza, M. A. Malik, R. W. Murray, *J. Am. Chem. Soc.* **2002**, *124*, 8958.
[45] M. C. Leopold, R. L. Donkers, D. Georganopoulou, M. Fisher, F. P. Zamborini, R. W. Murray, *Faraday Discuss.* **2004**, *125*, 63.
[46] N. Krasteva, I. Besnard, B. Guse, R. E. Bauer, K. Mullen, A. Yasuda, T. Vossmeyer, *Nano Lett.* **2002**, *2*, 551.
[47] Y. Joseph, B. Guse, A. Yasuda, T. Vossmeyer, *Sens. Actuators B* **2004**, *98*, 188.
[48] J. Im, A. Chandekar, J. E. Whitten, *Langmuir* **2009**, *25*, 4288–4292.
[49] E. García-Berríos, B. S. Brunschwig, T. Gao, M. D. Woodka, M. W. Ellsworth, S. Maldonado, N. S. Lewis, *J. Phys. Chem. C* **2010**, *114*, 21914.
[50] J. Guo, P. Pang, Q. Cai, *Sens. Actuators B* **2007**, *120*, 521.
[51] Y. Hatakeyama, M. Umetsu, S. Ohara, F. Kawadai, S. Takami, T. Naka, T. Adschiri, *Adv. Mater.* **2008**, *20*, 1122.
[52] M. D. Hanwell, S. Y. Heriot, T. H. Richardson, N. Cowlam, L. M. Ross, *Colloids Surf. A: Phys. Chem. Eng. Aspects* **2006**, *284–285*, 311.
[53] L.-P. Xu, S. Chen, *Chem. Phys. Lett.* **2009**, *468*, 222.
[54] E. Chow, T. R. Gengenbach, L. Wieczorek, B. Raguse, *Sens. Actuators B* **2010**, *143*, 704.
[55] F. J. Ibañez, F. P. Zamborini, *J. Am. Chem. Soc.* **2008**, *130*, 622.
[56] L. C. Brousseau, Q. Zhao, D. A. Shultz, D. L. Feldheim, *J. Am. Chem. Soc.* **1998**, *120*, 7645.
[57] D. L. Gittins, D. Bethell, D. J. Schiffrin, R. J. Nichols, *Nature* **2000**, *408*, 67.
[58] S.-J. Park, T. A. Taton, C. A. M. Mirkin, *Science* **2002**, *295*, 1503.
[59] C. Fang, Y. Fan, J. Kong, Z. Gao, N. Balasubramanian, *Anal. Chem.* **2008**, *80*, 9387.
[60] J. Turkevich, P. C. Stevenson, J. Hillier, *Discuss. Faraday Soc.* **1951**, 55.
[61] X. Huang, S. Neretina, M. A. El-Sayed, *Adv. Mater.* **2009**, *21*, 4880.
[62] D. I. Gittins, F. Caruso, *J. Phys. Chem. B* **2001**, *105*, 6846.
[63] G. Corthey, L. J. Giovanotti, J. M. Ramallo-Lopez, E. Zelaya, A. A. Rubert, G. A. Benitez, F. G. Requejo, M. H. Fonticelli, R. C. Salvarezza, *ACS Nano* **2010**, *4*, 3413.
[64] C. Vericat, M. E. Vela, G. Benitez, P. Carro, R. C. Salvarezza, *Chem. Soc. Rev.* **2010**, *39*, 1805.
[65] M. J. Hostetler, J. E. Wingate, C.-J. Zhong, J. E. Harris, R. W. Vachet, M. R. Clark, J. D. Londono, S. J. Green, J. J. Stokes, G. D. Wignall, G. L. Glish, M. D. Porter, N. D. Evans, R. W. Murray, *Langmuir* **1998**, *14*, 17.
[66] M. Brust, M. Walker, D. Bethell, D. J. Schiffrin, R. Whyman, *J. Chem. Soc., Chem. Commun.* **1994**, *7*, 801.
[67] Y. Joseph, I. Besnard, M. Rosenberger, B. Guse, H.-G. Nothofer, J. M. Wessels, U. Wild, A. Knop-Gericke, D. Su, R. Schlogl, A. Yasuda, T. Vossmeyer, *J. Phys. Chem. B* **2003**, *107*, 7406.
[68] M. J. Hostetler, A. C. Templeton, R. W. Murray, *Langmuir* **1999**, *15*, 3782.
[69] A. C. Templeton, M. J. Hostetler, E. K. Warmoth, S. Chen, C. M. Hartshorn, V. M. Krishnamurthy, M. D. E. Forbes, R. W. Murray *J. Am. Chem. Soc.* **1998**, *120*, 4845.
[70] C.-J. Zhong, W. X. Zheng, F. L. Leibowitz, H. H. Eichelberger, *Chem. Commun.* **1999**, 1211.
[71] L. Wang, J. Luo, M. J. Schadt, C.-J. Zhong, *Langmuir* **2009**, *26*, 618.
[72] H. Shiigi, S. Tokonami, H. Yakabe, T. J. Nagaoka, *J. Am. Chem. Soc.* **2005**, *127*, 3280.
[73] S. H. Brewer, W. R. Glomm, M. K. Knag, M. C. Johonson, S. Franzen, *Langmuir* **2005**, *21*, 9303.
[74] S. Tokonami, H. Shiigi, T. Nagaoka, *Electronanalysis* **2007**, *20*, 355.
[75] F. J. Ibañez, F. P. Zamborini, *Langmuir* **2006**, *22*, 9789.
[76] S. Tokonami, H. Shiigi, T. Nagaoka, *J. Electrochem. Soc.* **2008**, *115*, 105.
[77] Y. Joseph, N. Krasteva, I. Besnard, B. Guse, M. Rosenberger, U. Wild, A. Knop-Gericke, R. Schlogl, R. Krustev, A. Yasuda, T. Vossmeyer, *Faraday Discuss.* **2004**, *125*, 77.
[78] O. Harnack, I. Raible, A. Yasuda, T. Vossmeyer, *Appl. Phys. Lett.* **2005**, *86*, 034108.
[79] B. Raguse, E. C. Christopher, C. S. Barton, L. Wieczorek, *Anal. Chem.* **2007**, *79*, 7333.
[80] B. Abeles, *R. C. A. Review* **1975**, *36*, 594.
[81] R. H. Terrill, T. A. Postlethwaite, C.-H. Chen, C.-D. Poon, A. Terzis, A. Chen, J. E. Hutchison, M. R. Clark, G. Wignall, J. D. Londono, R. Superfine, M. Falvo, C. S. Johnson Jr., E. T. Samulski, R. W. Murray, *J. Am. Chem. Soc.* **1995**, *117*, 12537.
[82] P. Sheng, B. Abeles, *Phys. Rev. Lett.* **1972**, *28*, 34.
[83] F. Favier, E. C. Walter, M. P. Zach, T. Benter, R. M. Penner, *Science* **2001**, *293*, 2227.
[84] A. J. Bard, L. R. Faulkner, In *Electrochemical Methods, Fubdamentals, and Applications* (Ed. E. Swain), John Wiley and Sons, Inc., New York **2001**, p. 814.
[85] J. W. Grate, D. A. Nelson, R. Skaggs, *Anal. Chem.* **2003**, *75*, 1868.
[86] S. D. Evans, S. R. Johnson, Y. L. Cheng, T. Shen, *J. Mater. Chem.* **2000**, *10*, 183.
[87] M. P. Rowe, W. H. Steineker, E. T. Zellers, *Anal. Chem.* **2007**, *79*, 1164.
[88] G. Peng, U. Tisch, O. Adams, M. Hakim, N. Shehada, Y. Y. Broza, S. Billan, R. Abdah-Bortnyak, A. Kuten, H. Haick, *Nat. Nanotechnol.* **2009**, *4*, 669.
[89] G. Peng, M. Hakim, Y. Y. Broza, S. Billan, R. Abdah-Bortnyak, A. Kuten, U. Tisch, H. Haick, *Brit. J. Cancer* **2010**, *103*, 542.
[90] E. Dovgolevsky, U. Tisch, H. Haick, *Small* **2009**, *5*, 1158
[91] L. Wang, J. Luo, J. Yin, H. Zhang, J. Wu, X. Shi, E. Crew, Z. Xu, Q. Rendeng, S. Lu, M. Poliks, B. Sammakia, C.-J. Zhong, *J. Mater. Chem.* **2009**, *20*, 907.
[92] M. J. Schadt, W. Cheung, J. Luo, C.-J. Zhong, *Chem. Mater.* **2006**, *18*, 5147.
[93] F. L. Leibowitz, W. Zheng., M. M. Maye,C.-J. Zhong, *Anal. Chem.* **1999**, *71*, 5076.
[94] Y. Joseph, A. Peic, X. Chen, J. Michel, T. Vossmeyer, A. Yasuda, *J. Phys. Chem. C* **2007**, *111*, 12855.
[95] P. Pang, Z. Guo, S. Wu, Q. Cai, *Sens. Actuators B* **2006**, *114*, 799.
[96] Y. Joseph, B. Guse, T. Vossmeyer, A. Yasuda, *J. Phys. Chem. C* **2008**, *112*, 212507.
[97] N. Krasteva, Y. Fogel, R. E. Bauer, K. Mullen, Y. Joseph, A. Matsuzawa, T. Vossmeyer, *Adv. Funct. Mater.* **2007**, *17*, 881.
[98] M. Moreno, F. J. Ibañez, J. B. Jasinski, F. P. Zamborini, *J. Am. Chem. Soc.* **2011**, *113*, 4389.
[99] J.-P. Choi, R. W. Murray, *J. Am. Chem. Soc.* **2006**, *128*, 10496.

[100] E. Chow, J. Herrmann, C. S. Barton, B. Raguse, L. Wieczorek, *Anal. Chim. Acta* **2009**, *632*, 135.
[101] B. Raguse, C. S. Barton, K. H. Müller, E. Chow, L. Wieczorek, *J. Phys. Chem. C* **2009**, *113*, 15390.
[102] D. L. Feldheim, *Nature* **2000**, *408*, 45.
[103] S. Tokonami, M. Iwamoto, K. Hashiba, H. Shiigi, T. Nagaoka, *Solid State Ionic* **2006**, *177*, 2317.
[104] W. Kruppa, M. G. Ancona, R. W. Rendell, A. W. Snow, E. E. Foos, R. Bass, *Appl. Phys. Lett.* **2008**, *88*, 053120.
[105] E. L. Covington, R. W. Turner, C. Kurdak, M. P. Rowe, C. Xu, E. T. Zellers, *IEEE Sensors* **2008**, 102.
[106] J. F. Parker, C. A. Fields-Zinna, R. W. Murray, *Acc. Chem. Res.* **2010**, *43*, 1289.
[107] C. J. Murphy, T. K. Sau, A. M. Gole, C. J. Orendorff, J. Gao, L. Gou, S. E. Hunyadi, T. Li, *J. Phys. Chem. B* **2005**, *109*, 13857.
[108] J. Kong, M. G. Chapline, H. Dai, *Adv. Mater.* **2001**, *13*, 1384.
[109] N. R. Jana, L. Gearheart, C. J. Murphy, *J. Phys. Chem. B* **2001**, *105*, 4065.
[110] N. Krasteva, R. Krustev, A. Yasuda, T. Vossmeyer, *Langmuir* **2003**, *19*, 7754.
[111] N. Krasteva, B. Guse, I. Besnard, A. Yasuda, T. Vossmeyer, *Sens. Actuators B* **2003**, *92*, 137.

Received: December 10, 2010
Revised: March 31, 2011
Published online: November 4, 2011

